

**SYNTHESIS OF NITROGEN-DOPED CARBON DOTS
FROM AROMATIC AMINO ACIDS**



Mr. Nattapon Siengdung

จุฬาลงกรณ์มหาวิทยาลัย
CHULALONGKORN UNIVERSITY

A Thesis Submitted in Partial Fulfillment of the Requirements
for the Degree of Master of Science in Chemistry
Department of Chemistry
FACULTY OF SCIENCE
Chulalongkorn University
Academic Year 2020
Copyright of Chulalongkorn University

การสังเคราะห์คาร์บอนคอตที่เจือด้วยไนโตรเจนจากกรดอะมิโนที่มีวงแอโรแมติก



วิทยานิพนธ์นี้เป็นส่วนหนึ่งของการศึกษาตามหลักสูตรปริญญาวิทยาศาสตรมหาบัณฑิต

สาขาวิชาเคมี ภาควิชาเคมี

คณะวิทยาศาสตร์ จุฬาลงกรณ์มหาวิทยาลัย

ปีการศึกษา 2563

ลิขสิทธิ์ของจุฬาลงกรณ์มหาวิทยาลัย

Thesis Title SYNTHESIS OF NITROGEN-DOPED CARBON
 DOTS FROM AROMATIC AMINO ACIDS
By Mr. Nattapon Siengdung
Field of Study Chemistry
Thesis Advisor Assistant Professor PROMPONG PIENPINIJTHAM,
 Ph.D.

Accepted by the FACULTY OF SCIENCE, Chulalongkorn University in
Partial Fulfillment of the Requirement for the Master of Science

..... Dean of the FACULTY OF
 SCIENCE
(Professor POLKIT SANGVANICH, Ph.D.)

THESIS COMMITTEE

..... Chairman
(Professor VUDHICHAJ PARASUK, Ph.D.)
..... Thesis Advisor
(Assistant Professor PROMPONG PIENPINIJTHAM,
Ph.D.)
..... Examiner
(Professor SUMRIT WACHARASINDHU, Ph.D.)
..... Examiner
(Assistant Professor SAKULSUK UNARUNOTAI,
Ph.D.)
..... External Examiner
(Associate Professor Pimthong Thongnopkun, Ph.D.)

จุฬาลงกรณ์มหาวิทยาลัย
CHULALONGKORN UNIVERSITY

นัฐพล เสียงดั่ง : การสังเคราะห์คาร์บอนดอตที่เจือด้วยไนโตรเจนจากกรดอะมิโนที่มีวงแอมโรแมติก. (SYNTHESIS OF NITROGEN-DOPED CARBON DOTS FROM AROMATIC AMINO ACIDS) อ.ที่ปรึกษาหลัก : ผศ. ดร.พร้อมพงศ์ เพียรพิณิจธรรม

คาร์บอนดอตที่เจือด้วยไนโตรเจน (nitrogen-doped carbon dots, NCDs) สามารถสังเคราะห์ขึ้นได้จากกรดอะมิโนด้วยวิธีไฮโดรเทอร์มัลภายใต้สภาวะกรด สารตั้งต้นที่ใช้ในการสังเคราะห์ได้แก่ แอล-ฮิสทีดีน (L-histidine) แอล-ฟีนิลอะลานีน (L-phenylalanine) แอล-ไทโรซีน (L-tyrosine) แอล-ทริปโตเฟน (L-tryptophan) และไกลซีน (glycine) โดย NCDs ที่สังเคราะห์ได้จากสารตั้งต้นดังกล่าวระบุชื่อเป็น His-NCDs, Phe-NCDs, Tyr-NCDs, Trp-NCDs และ Gly-NCDs ตามลำดับ การศึกษาสมบัติเชิงแสง โครงสร้างทางเคมี และสัณฐานวิทยาของ NCDs ทำโดยใช้วิธีการทางไมโครสโคปีและสเปกโทรสโคปี ผลการทดลองแสดงให้เห็นว่า NCDs ทุกชนิดมีลักษณะอนุภาคเป็นทรงกลม มีเส้นผ่านศูนย์กลางเฉลี่ย 4.11 ± 1.20 นาโนเมตร สามารถจำแนก NCDs ออกได้เป็นสองกลุ่มโดยใช้ค่าช่องว่างระหว่างระดับพลังงานของออร์บิทัลเชิงโมเลกุลสูงสุดที่มีอิเล็กตรอนบรรจุอยู่ (highest occupied molecular orbitals, HOMO) กับออร์บิทัลเชิงโมเลกุลต่ำสุดที่ไม่มีอิเล็กตรอนบรรจุอยู่ (lowest unoccupied molecular orbitals, LUMO) ที่ได้จากฟลูออเรสเซนซ์สเปกโทรสโคปีเป็นเกณฑ์ โดยกลุ่มหนึ่งประกอบไปด้วย Phe-NCDs และ Gly-NCDs ซึ่งมีช่องว่างระหว่างพลังงานของ HOMO กับ LUMO ประมาณ 5 อิเล็กตรอนโวลต์ และอีกกลุ่มหนึ่งประกอบไปด้วย His-NCDs, Tyr-NCDs และ Trp-NCDs ซึ่งมีช่องว่างระหว่างระดับพลังงานของ HOMO กับ LUMO ประมาณ 4 อิเล็กตรอนโวลต์ สเปกตรัมฟลูออเรสเซนซ์ฟลูออเรสเซนซ์สเปกโทรสโคปีของ Gly-NCDs มีปริมาณของหมู่ฟังก์ชันบนพื้นผิวน้อยกว่า NCDs ชนิดอื่น ทำให้สามารถตั้งสมมติฐานได้ว่า Gly-NCDs มีศูนย์กลางการเปล่งแสงฟลูออเรสเซนซ์คือบริเวณแกนของอนุภาค (core atate) เนื่องจากมีค่าช่องว่างระหว่างระดับพลังงานของ HOMO กับ LUMO สูง และมีปริมาณหมู่ฟังก์ชันบนพื้นผิวน้อยกว่า นอกจากนี้ยังสามารถสันนิษฐานได้ว่าศูนย์กลางการเปล่งแสงฟลูออเรสเซนซ์ของ Phe-NCDs นั้นเหมือนกับ Gly-NCDs เนื่องจาก Phe-NCDs มีช่องว่างระหว่างระดับพลังงานของ HOMO กับ LUMO ที่ใกล้เคียงกับ Gly-NCDs สเปกตรัมฟลูออเรสเซนซ์ฟลูออเรสเซนซ์สเปกโทรสโคปีของ His-NCDs, Tyr-NCDs และ Trp-NCDs แสดงให้เห็นว่าอนุภาคดังกล่าวมีปริมาณของหมู่ฟังก์ชันบนพื้นผิวอนุภาคที่มากกว่า จึงสันนิษฐานได้ว่าศูนย์กลางการเปล่งแสงฟลูออเรสเซนซ์ของ His-NCDs, Tyr-NCDs และ Trp-NCDs คือบริเวณพื้นผิวของอนุภาค (surface state) อัตราส่วนระหว่างดีแบนด์และจีแบนด์ (I_D/I_G) สามารถหาได้จากสเปกตรัมรามาน ผลการทดลองแสดงให้เห็นว่า NCDs ที่สังเคราะห์ขึ้นจากกรดอะมิโนที่มีวงแอมโรแมติก ยกเว้น Tyr-NCDs มีค่า I_D/I_G ที่ต่ำกว่าค่าดังกล่าวของ Gly-NCDs อย่างมีนัยสำคัญ ความเป็นแกรไฟติก (graphitic) ที่บริเวณแกนกลางของอนุภาคที่สูงกว่าอาจได้รับผลมาจากวงแอมโรแมติกในโครงสร้างของกรดอะมิโน อย่างไรก็ตาม Tyr-NCDs มีค่า I_D/I_G ที่มากที่สุด ซึ่งการที่มีค่าหน้าที่แกนกลางของอนุภาคที่มากกว่าอาจเป็นผลมาจากการรบกวนของผลของความเกะกะ (steric effect) ของหมู่ไฮดรอกซิลระหว่าง

สาขาวิชา เคมี ลายมือชื่อนิสิต

ปีการศึกษา 2563 ลายมือชื่อ อ.ที่ปรึกษาหลัก

6071936823 : MAJOR CHEMISTRY

KEYWORD Nitrogen-doped carbon dots, Hydrothermal, aromatic amino acids
D:

Nattapon Siengdung : SYNTHESIS OF NITROGEN-DOPED CARBON DOTS FROM AROMATIC AMINO ACIDS. Advisor: Asst. Prof. PROMPONG PIENPINIJTHAM, Ph.D.

Nitrogen-doped carbon dots (NCDs) were synthesized from amino acids via the hydrothermal method under an acidic condition. L-histidine, L-phenylalanine, L-tyrosine, L-tryptophan, and glycine were used as a precursor which NCDs synthesized from those precursors were labeled as His-NCDs, Phe-NCDs, Tyr-NCDs, Trp-NCDs, and Gly-NCDs, respectively. Spectroscopic and microscopic characterizations were operated to investigate optical properties, chemical structures, and morphologies of NCDs. The results show that all NCDs show a spherical shape with an average diameter of 4.11 ± 1.20 nm. Their energy gap between the highest occupied molecular orbitals (HOMO) and the lowest unoccupied molecular orbitals (LUMO) obtained from fluorescence spectroscopy can be used to classify NCDs into two groups. The first group is Gly-NCDs and Phe-NCDs which their HOMO-LUMO energy gap is ~ 5 nm. Furthermore, the other group is His-NCDs, Tyr-NCDs, and Trp-NCDs which their HOMO-LUMO energy gap is ~ 4 nm. Gly-NCDs show lower content of surface functional groups than other NCDs. From the HOMO-LUMO energy gap and the low content of surface functional groups of Gly-NCDs, their fluorescence emission center might be a core state. The fluorescence emission center of Phe-NCDs was assumed to be like Gly-NCDs due to their similar HOMO-LUMO energy gap. His-NCDs, Tyr-NCDs, and Trp-NCDs show higher content of surface functional groups. Hence, the fluorescence emission center of His-NCDs, Tyr-NCDs, and Trp-NCDs was assumed to be a surface state. I_D/I_G values of NCDs were obtained from Raman spectra. The results show that NCDs synthesized from aromatic amino acids, except Tyr-NCDs, show significantly lower I_D/I_G than Gly-NCDs. The aromatic sidechain of precursors might cause higher graphitic content in the carbon core of NCDs. However, Tyr-NCDs show the highest I_D/I_G . A larger defect area in the graphitic carbon core of Tyr-NCDs might be altered by the steric effect of a hydroxyl group during polymerization and carbonization.

Field of Study: Chemistry

Student's Signature

Academic Year: 2020

Advisor's Signature

Year:

.....

ACKNOWLEDGEMENTS

I would like to express my most profound appreciation to my advisor, Assistant Professor Dr. Prompong Pienpinijtham. His supports are priceless to me, whether in the research, studying, or any financial supports. This research project cannot succeed without his precious guidance and feedback. For four years of my master's study, it is like as I am driving a car along a road with plenty of sharp stones. He is an express mechanic who repairs my car every time that my car is broken. Honestly, I could not have imagined having a better advisor and mentor for my study.

Moreover, I would like to extend my special thanks to Professor Dr. Sanong Ekgasit for his financial support and valuable suggestion, and Associate Professor Dr. Kanet Wongravee for some guidance and his chit-chat talk almost every morning. Additionally, I would like to sincerely thank my colleagues at the Sensor Research Unit (SRU), especially Miss Thanyada Sukmanee, who always encourage and motivate me and always share me ground coffee, and Miss Sureerat Makmuang, Miss Wisansaya Jaikandee, Miss Piboonwan Insiti, and Mr. Boonphop Chaisrikhwun, who usually stay with me when I have to stay at the office at late night. Furthermore, I also wish to thank Miss Thayida Manuwong for her management of all bills and documents in the office.

I would like to show my appreciation to the Development and Promotion of Science and Technology Talents (DPST) project for financial support of my master's study for three years and support me to attend the international conference in Belgium, which is a priceless experience. Besides, I gratefully acknowledge the financial support from the National Nanotechnology Center (NANOTEC), NSTDA, Ministry of Science and Technology, Thailand, through its Research Network NANOTEC (RNN) program.

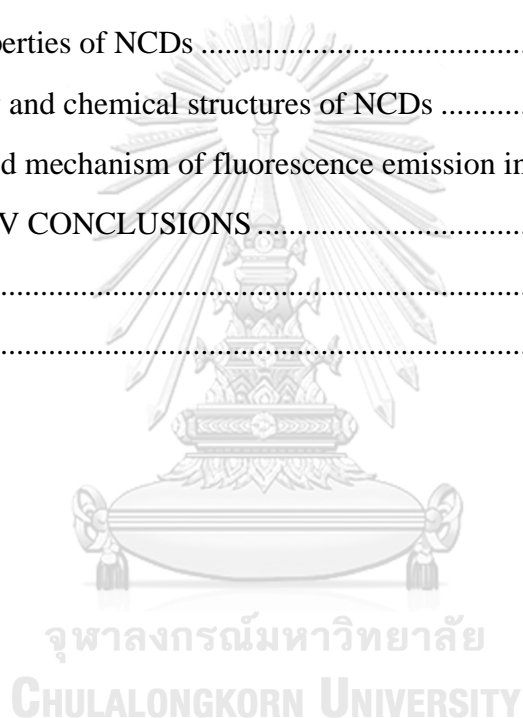
Above all, I would also like to extend my deepest gratitude to my family for everything. They always encourage me every time I am tired, console me every time I am sad, appreciate me every time I succeed, and pay me every time I am asking for. Without them, this journey would not even start.

Nattapon Siengdung

TABLE OF CONTENTS

	Page
.....	iii
ABSTRACT (THAI)	iii
.....	iv
ABSTRACT (ENGLISH)	iv
ACKNOWLEDGEMENTS	v
TABLE OF CONTENTS	vi
LIST OF TABLE	8
LIST OF FIGURES	9
LIST OF ABBREVIATIONS AND SYMBOLS	12
1. CHAPTER I INTRODUCTION	14
1.1 Problems and backgrounds	14
1.2 Objectives	16
1.3 Scope of this work	16
1.4 The benefit of this research.....	17
2. CHAPTER II LITERATURE REVIEW	18
2.1 Carbon dots and their classification.....	18
2.2 Synthesis and characterization of CDs	20
2.3 Fluorescence phenomena.....	21
2.4 Structure and properties of carbon dots	22
2.5 Fluorescence mechanisms of carbon dots.....	23
2.5.1 Quantum confinement effect (QCE)	23
2.5.2 Surface defect state.....	25
2.5.3 Molecular fluorescence	27
2.5.4 Heteroatom doping	28
2.6 Nitrogen-doped carbon dots.....	28

3.	CHAPTER III EXPERIMENTAL SECTION	30
3.1	Chemicals.....	30
3.2	Synthesis of nitrogen-doped carbon dots.....	30
3.3	Characterizations	31
3.3.1	Optical properties characterizations	31
3.3.2	Morphological characterization.....	32
3.3.3	Chemical structure characterization	32
4.	CHAPTER IV RESULTS AND DISCUSSION	34
4.1	Optical properties of NCDs	34
4.2	Morphology and chemical structures of NCDs	41
4.3	The proposed mechanism of fluorescence emission in NCDs	48
5.	CHAPTER V CONCLUSIONS	53
	REFERENCES	55
	VITA.....	66



LIST OF TABLE

	Pages
Table 4.1 λ_{ex} , λ_{em} and ΔE obtained from fluorescence spectra of each NCDs.....	39
Table 4.2 Relative quantum yield (QY) of each NCDs.....	41
Table 4.3 Average diameter of each NCDs.....	42
Table 4.4 FTIR band assignments of different NCDs.....	44
Table 4.5 Ratio between I_D and I_G of each NCDs.....	47

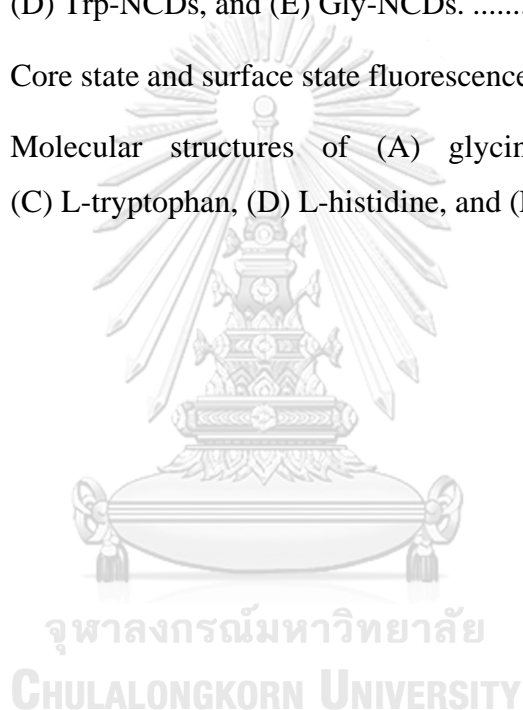


LIST OF FIGURES

		Pages
Figure 2.1	Carbon dots (CDs) are classified into three types: graphene quantum dots (GQDs), carbon nanodots (CNDs), and polymer dots (PDs). Reprinted with permission from ref. [18], Copyright 2015, Springer.	19
Figure 2.2	Diagram to describe the reaction process of HTCP to prepare CPDs by the “bottom-up” route. Reprinted with permission from ref. [20], Copyright 2019, American Chemical Society.....	19
Figure 2.3	Diagram of top-down and bottom-up synthesis of CDs. Reprinted with permission from ref. [18], Copyright 2015, Springer.....	20
Figure 2.4	Jablonski diagram of fluorescence and phosphorescence	21
Figure 2.5	(A)-(C) TEM images (top) of CDs synthesized in water, glycerol, and DMF; and their corresponding size histograms (bottom). (D) Absorption and fluorescence emission spectra of CDs were synthesized in water, glycerol, and DMF, respectively, at 360, 420, and 540 nm excitations. Reprinted with permission from ref. [34], Copyright 2017, John Wiley and Sons.....	24
Figure 2.6	(A) Synthesis of CDs in Ding’s research. (B) Images that were taken under 365 nm UV light and (C) fluorescence emission spectra of each fraction of CDs. (D) influence of the degree of surface oxidation on their HOMO and LUMO gap. Reprinted with permission from ref. [40], Copyright 2016, American Chemical Society.	26
Figure 2.7	Schematic presentation of CDs synthesis in Song’s research. Reprinted with permission from ref. [18], Copyright 2019, Springer.	27

Figure 2.8	Representation for the fluorescent mechanism of O-CDs, N-CDs, and N,S-CDs. 1) Electrons excited from the ground state and trapped by the surface states; 2) excited electrons return to the ground state via a non-radiative route; 3) excited electrons return to the ground state via a radiative route. Reprinted with permission from ref. [52], Copyright 2013, John Wiley and Sons.29
Figure 2.9	Schematic presentation of tunable fluorescence emission with increasing nitrogen content in the graphitic framework. Reprinted with permission from ref. [55], Copyright 2017, American Chemical Society.....29
Figure 4.1	UV-visible spectra of synthesized NCDs34
Figure 4.2	Fluorescence emission spectra using various excitation wavelength from 300–400 nm with an increment of 10 nm collected from (A) His-NCDs, (B) Phe-NCDs, (C) Tyr-NCDs, (D) Trp-NCDs, and (E) Gly-NCDs.35
Figure 4.3	Plots between the excitation wavelength and emission wavelength of (A) His-NCDs, (B) Phe-NCDs, (C) Tyr-NCDs, (D) Trp-NCDs, and (E) Gly-NCDs.36
Figure 4.4	Plots between maximum emission intensities and their corresponding excitation wavelength of (A) His-NCDs, (B) Phe-NCDs, (C) Tyr-NCDs, (D) Trp-NCDs, and (E) Gly-NCDs37
Figure 4.5	Plots between excitation wavelength and emission wavelength of (A) Phe-NCDs and (C) Gly-NCDs. Plots between excitation wavelength and emission intensity of (B) Phe-NCDs and (D) Gly-NCDs38
Figure 4.6	The energy gap between HOMO and LUMO, and the width of the additional interband of each NCDs.....40

Figure 4.7	TEM images of (A) His-NCDs, (B) Phe-NCDs, (C) Tyr-NCDs, (D) Trp-NCDs, and (E) Gly-NCDs41
Figure 4.8	Size distribution of NCDs.....42
Figure 4.9	FTIR spectra of dialyzed NCDs43
Figure 4.10	FTIR spectra of Tyr-NCDs, Trp-NCDs, and Gly-NCDs in the range of 1750–1250 cm^{-1}45
Figure 4.11	Raman spectra of (A) His-NCDs, (B) Phe-NCDs, (C) Tyr-NCDs, (D) Trp-NCDs, and (E) Gly-NCDs.46
Figure 4.12	Core state and surface state fluorescence emission center48
Figure 4.13	Molecular structures of (A) glycine, (B) L-phenylalanine, (C) L-tryptophan, (D) L-histidine, and (E) L-tyrosine50



LIST OF ABBREVIATIONS AND SYMBOLS

C	: Carbon
CA	: Citric acid
DMF	: Dimethylformamide
H	: Hydrogen
N	: Nitrogen
O	: Oxygen
CDs	: Carbon dots
NCDs	: Nitrogen-doped carbon dots
SQDs	: Semiconductor quantum dots
GQDs	: Graphene quantum dots
CNDs	: Carbon nanodots
CNTs	: Carbon nanotubes
SWCNTs	: Single-walled carbon nanotubes
PDs	: Polymer dots
CPDs	: Carbonized polymer dots
°C	: Degree Celsius
hr	: hour
nm	: nanometer
HOMO	: Highest occupied molecular orbital
LUMO	: Lowest unoccupied molecular orbital
His-NCDs	: Nitrogen-doped carbon dots synthesized from L-histidine
Phe-NCDs	: Nitrogen-doped carbon dots synthesized from L-phenylalanine
Tyr-NCDs	: Nitrogen-doped carbon dots synthesized from L-tyrosine
Trp-NCDs	: Nitrogen-doped carbon dots synthesized from L-tryptophan
Gly-NCDs	: Nitrogen-doped carbon dots synthesized from L-glycine
FTIR	: Fourier-transform infrared
TEM	: Transmission electron microscopy
UV	: Ultraviolet
QY	: Quantum yield
cps	: Count per second
a.u.	: Arbitrary unit
λ_{ex}	: Excitation wavelength inducing NCDs to emit fluorescence at the

	maximum intensity
λ_{em}	: Emission wavelength at the maximum emission intensity
E_{ex}	: Excitation energy
E_{em}	: Energy released in the radiation relaxation step
ΔE	: The difference of excitation energy and energy released in the radiative relaxation step
E	: Energy
h	: Planck's constant
λ	: wavelength
c	: velocity of light
<i>et al.</i>	: et al ii, in Latin meaning "and others"
QY_s	: Quantum yield of a sample
QY_r	: Quantum yield of a reference
n_s	: a refractive index of a media of a sample
n_r	: a refractive index of a media of a reference
m_s	: a gradient obtained from the linear trendline created from the plot between UV-visible absorption and integrated fluorescence emission intensity of a sample
m_r	: a gradient obtained from the linear trendline created from the plot between UV-visible absorption and integrated fluorescence emission intensity of a reference
QHS	: Quinine hemisulfate monohydrate
rpm	: round per minute
QCE	: Quantum confinement effect

CHAPTER I

INTRODUCTION

1.1 Problems and backgrounds

Carbon dots (CDs) are spherical carbon nanoparticles whose size is smaller than 10 nm [1]. Fluorescence, photobleaching resistance, and high biocompatibility are their attractive properties that make CDs useful in various applications such as bioimaging [2], biosensing [3], chemosensing [4], and catalysis [5]. Carbon dots were coincidentally discovered by Xu and co-workers in 2004 during the gel-electrophoresis purification of their single-walled carbon nanotubes (SWCNTs) synthesized from arc-discharge soot [6].

CDs can be synthesized *via* two approaches: the top-down and bottom-up. The top-down method is based on the fragmentation of bulk carbon materials such as graphite, graphene, carbon nanotubes (CNTs), carbon black, and coal [1, 7]. On the other hand, the bottom-up method is based on the carbonization of small molecules, such as carbohydrates, organic acids and amine, and polymer precursors [1, 7].

The fluorescence properties of CDs are still lower than those of semiconductor quantum dots (SQDs) [8]. Bare CDs are composed of carbon (C) and oxygen (O) which their emission wavelength is usually blue, and quantum yield is low [9]. Doping with heteroatoms is a way which can adjust the fluorescence of CDs, whether it be emission wavelength and quantum yield [9, 10]. Doped heteroatoms can be embedded into graphitic carbon core or at the surface functional groups.

The most studied and the highest potential doping system is nitrogen-doped carbon dots (NCDs) due to five valence electrons of N and their similar atomic size between N and C [10-13]. NCDs can be synthesized *via* both bottom-up and top-down methods [7]. For the top-down methods of NCDs, bulk carbon materials must be nitrogen-doped before going in the fragmentation process, or those undoped bulk carbon materials must be fragmented under N-rich conditions [7]. For example, Li *et al.* [14] synthesized NCDs by oxidative fragmentation of N-doped graphene using concentrated H₂SO₄ and HNO₃ for 30 h cooperated with ultrasonication.

The bottom-up synthesis of NCDs can be done using co-reactants: carbonization sources and N-containing compounds [7]. For example, Zhai and co-workers synthesized NCDs by microwave-assisted pyrolysis using citric acid (CA) as a carbon source and 1,2-ethylenediamine (EDA) as a N dopant [15]. Moreover, NCDs can be bottom-up synthesized using single N-containing reactants such as amines, amides, and amino acids [7].

Amino acids are interesting molecular precursors for NCDs synthesis because of their high natural abundance, non-toxicity, and non-pollutant. In recent years, there are many pieces of research about NCDs synthesized from amino acids. Huang and co-workers [16] synthesized NCDs from histidine using a microwave-assisted hydrothermal method without any acid or alkali. Their synthesized NCDs showed a diameter of 2-5 nm with excitation-dependent fluorescent behavior. Moreover, Pei and co-workers [17] synthesized NCDs using the hydrothermal method under the acidic condition from three amino acids: serine, histidine, and cystine. The results show that their NCDs were spherical with a diameter of 2.5-4.7 nm. They found that molecular structures of precursors, reaction temperature, and reaction time could

affect particles size. All synthesized NCDs showed excitation-dependent fluorescence emission. Choi and co-workers synthesized blu-luminescent NCDs from lysine using the microwave-assisted method. They proposed that microwaves could induce lysine to form branched polylysine *via* polyamidation. 6-aminohexanoic acid and glycine were used as precursors of NCDs to compare with lysine-synthesized NCDs. The results show that NCDs could not be produced from 6-aminohexanoic acid and glycine because they could not form a branched polymer and were further carbonized to be NCDs like in a lysine-based system.

In this research, NCDs were synthesized from four aromatic amino acids: L-histidine, L-phenylalanine, L-tyrosine, and L-tryptophan. Hydrothermal under an acidic condition at a specific reaction temperature and time was applied to all precursors. Those NCDs were compared with NCDs synthesized from glycine. Optical properties, morphologies, and chemical structures of NCDs synthesized from each precursor were compared to observe the influence of the molecular structure of precursors on the properties and structures of synthesized NCDs.

จุฬาลงกรณ์มหาวิทยาลัย
CHULALONGKORN UNIVERSITY

1.2 Objectives

1. To synthesize NCDs from aromatic amino acids
2. To characterize synthesized NCDs

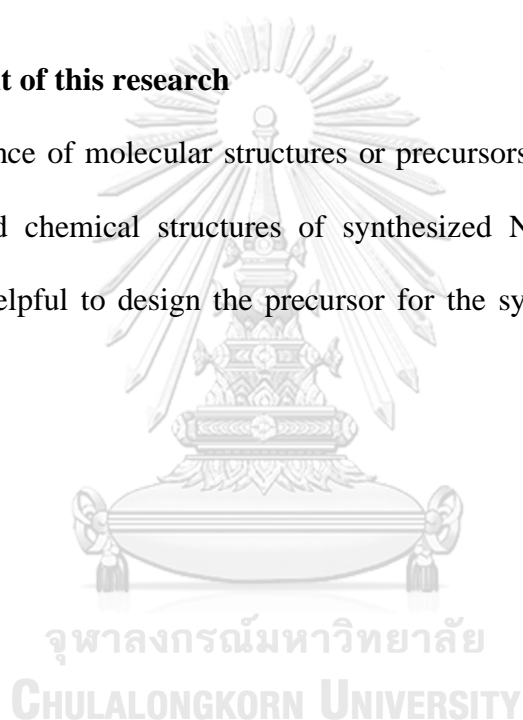
1.3 Scope of this work

1. To synthesize NCDs from L-histidine, L-phenylalanine, L-tyrosine, L-tryptophan, and glycine using hydrothermal method under an acidic condition at specific reaction temperature and time.

2. To spectroscopic and microscopic characterize synthesized NCDs
3. To compare optical properties, morphologies, and chemical structures of NCDs synthesized from each amino acid.
4. To investigate the influence of aromatic sidechains and heteroatom on the optical properties, morphologies, and chemical structures of synthesized NCDs.

1.4 The benefit of this research

The influence of molecular structures or precursors on the optical properties, morphologies, and chemical structures of synthesized NCDs investigated in this research can be helpful to design the precursor for the synthesis of NCDs with the expected features.



CHAPTER II

LITERATURE REVIEW

2.1 Carbon dots and their classification

Carbon materials which at least one dimension is smaller than 10 nm in size, could be called carbon dots (CDs) [18]. Most CDs are composed of at least 70% wt. of carbon with nitrogen (N) or oxygen (O) atoms in the functional groups located on the surface [18, 19]. Moreover, they display intrinsic fluorescence properties [19]. CDs can be classified by shape and crystallinity into four types: Graphene quantum dots (GQDs), carbon quantum dots (CQDs), carbon nanodots (CNDs), and polymer dots (PDs) [19]. GQDs are composed of several layers of graphenes that N- or O-based functional groups located at the edge. They are anisotropic with lateral dimension more than longitudinal. Quasi-spherical CDs with and without crystallinity are classified as CQDs and CNDs, respectively. PDs can be obtained from the aggregation or cross-linking of polymer chains [18, 19].

However, the aggregated or cross-linked might be carbonized to form carbonized polymer dots (CPDs), which their boundary between carbon core and polymer is not clear. The novel perspective in the classification of CDs, carbonized polymer dots (CPDs), has been exhibited in 2019 by Tao and colleagues [20]. The concept of CPDs classifies CDs by the carbonization level. Some synthetic route, especially hydrothermal and solvothermal, produce CDs with significant

heterogeneity. Different synthetic factors such as temperature and time tend to produce CDs with different ratio of amorphous and crystalline regions.

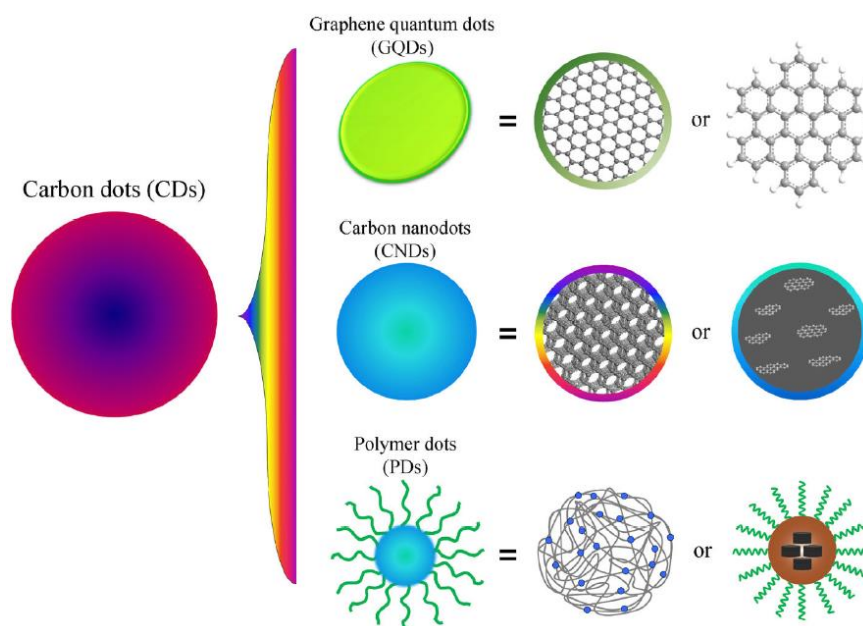


Figure 2.1 Carbon dots (CDs) are classified into three types: graphene quantum dots (GQDs), carbon nanodots (CNDs), and polymer dots (PDs). Reprinted with permission from ref. [18], Copyright 2015, Springer.

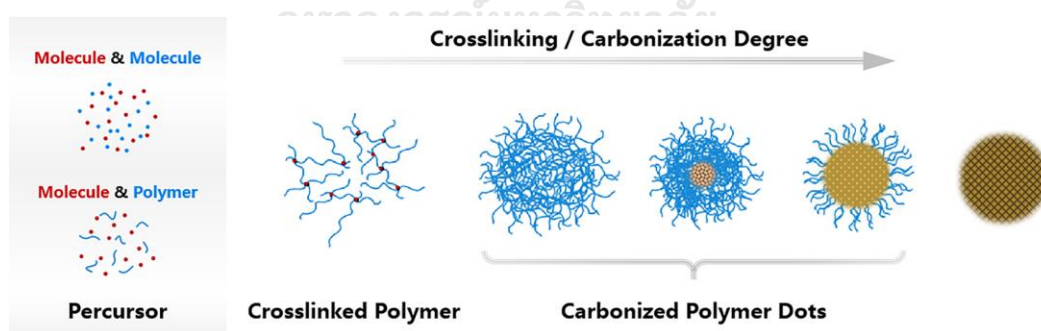


Figure 2.2 Diagram to describe the reaction process of HTCP to prepare CPDs by the “bottom-up” route. Reprinted with permission from ref. [20], Copyright 2019, American Chemical Society.

2.2 Synthesis and characterization of CDs

The essential criteria to classify the synthetic route of CDs is how they form. The synthesis of CDs can be classified into two routes: a top-down and bottom-up synthesis. For top-down synthesis, bulk carbon materials with an sp^2 carbon framework (such as graphenes, graphites, carbon nanotubes, carbon fibres and carbon soot [21]) will be cut into small CDs *via* various methods such as chemical and electrochemical oxidation [22, 23], arc discharge [6] and laser ablation [24]. On the other hand, bottom-up synthesis always starts with molecular precursors, in which carbon is the main component (such as organic molecules and polymers). Precursors in bottom-up synthesis can be citric acid, amino acids, polyethylene glycol, proteins, *etc.* Hydrothermal, solvothermal, and pyrolysis [25] are frequently used. This part will focus on a bottom-up synthesis because it is the primary method in this research.

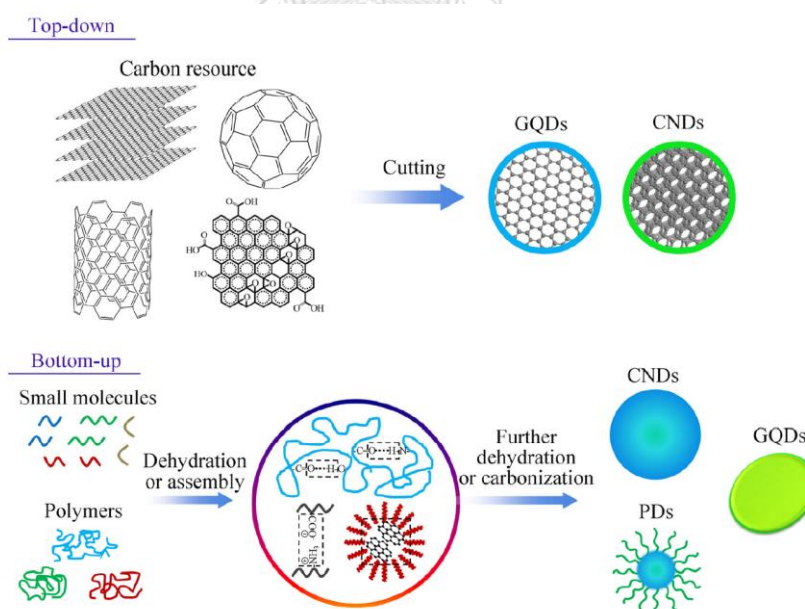


Figure 2.3 Diagram of top-down and bottom-up synthesis of CDs. Reprinted with permission from ref. [18], Copyright 2015, Springer.

2.3 Fluorescence phenomena

Fluorescence is one of the photoluminescence phenomena, which can be described with the Jablonski diagram. S_0 , S_1 , S_2 , and T_1 is denoting to ground state, first singlet excited state, second singlet excited state, and first triplet excited state, respectively. In each state, composed of many sublevels of vibrational energy states. Electrons in S_0 will be excited by photons to S_1 or S_2 . Then, they try to release their energy and back to S_0 .

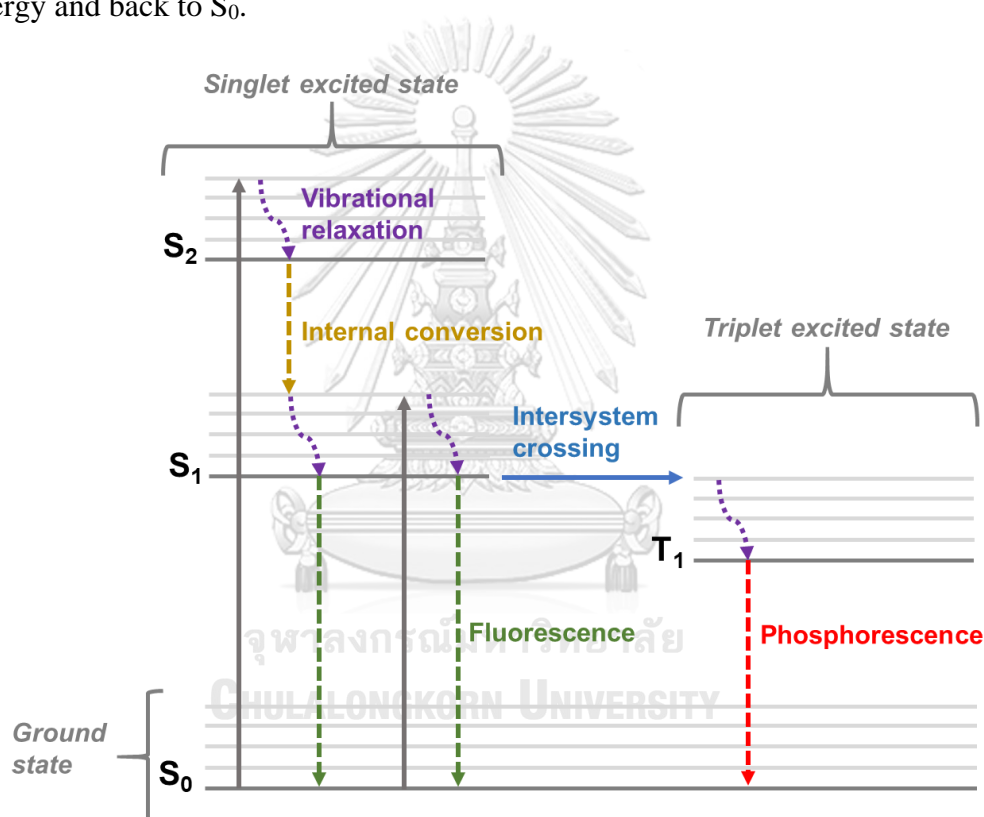


Figure 2.4 Jablonski diagram of fluorescence and phosphorescence

First, electrons from the highest vibrational energy level of each excited state are rapidly relaxing to the lowest vibrational energy level. This relaxation is called vibrational relaxation. Then, electrons from S_2 is moving to S_1 by internal conversion. There are two processes that can be done by electrons in S_1 . If those electrons go back to S_0 directly, this radiative relaxation is called fluorescence. However, electrons from

S_1 can be transferred through the intersystem crossing to T_1 , and the radiative relaxation of electrons from T_1 to S_0 is called phosphorescence [26].

2.4 Structure and properties of carbon dots

Carbon dots were frequently reported as a partially oxidized carbon material because there are hydroxyl, epoxy/ether, carbonyl, carboxylic acid on their surface [27]. Raman spectroscopy can be used for structure determination. Essential bands that should be observed from Raman spectra are D and G bands. D band attributes to breathing modes, which are assigned to the defect of graphitic domains, while G band arising from the E_{2g} vibrational modes of aromatic domains [27]. The integrated intensity ratio between the disordered D and crystalline G band (I_D/I_G) shows how amorphous or graphitic level those CDs are. Moreover, high-resolution transmission electron microscopy (HRTEM) can be used to determine the degree of oxidation of CDs. The interlayer spacing obtained from HRTEM images can be increased due to anchored hydroxyl, epoxy/ether, carbonyl, and carboxylic acid groups on their surface [27]. The crystallinity of CDs can be observed from the X-ray diffraction (XRD) pattern. A broad diffraction peak centered at ca. 23° usually observed. Broad diffraction peak is due to their small size [28, 29].

Significant optical properties of CDs are UV-visible absorption and photoluminescent behaviors. CDs always show two essential absorption bands in UV-visible spectra. The absorption band in the UV region is assigned to the $\pi-\pi^*$ transition of C=C bonds. The absorption tail, which can be extended out into the visible region, is assigned to the $n-\pi^*$ transition of C=O bonds/or others [27]. The attractive optical properties of CDs are their photoluminescence properties. Even the

mechanism of photoluminescence emission of CDs is still debated, and further systematic investigation is necessary; however, it is believed that quantum confinement effect (QCE), surface defect state, molecular fluorescence, and heteroatoms doping can affect the photoluminescence emission [9].

The other attractive property of CDs is their toxicity. CDs have been reported to there is low toxicity and highly biocompatible. Kang and Liu *et al.* used CDs as an *in vivo* fluorescence probe in live mice and further study the biodistribution of CDs. The results show that CDs could be accumulated in the reticuloendothelial system and kidney and gradually excreted by the kidney and gastrointestinal system [30].

2.5 Fluorescence mechanisms of carbon dots

2.5.1 Quantum confinement effect (QCE)

Quantum confinement effect (QCE) will be applied when there is a sizeable sp^2 -carbon framework with few surface functional groups, and their size is smaller than Bohr's exciton radius. The bandgap between the highest occupied molecular orbital (HOMO) and the lowest unoccupied molecular orbitals (LUMO), induced by conjugated π -domains at the carbon core, is considered a center of fluorescence emission [31-33]. The separation of valence and conduction bands results from the confined size of conjugated π -domains [9]. The size of conjugated π -domains affects the fluorescence emission color: larger conjugated π -domains, longer emission wavelength; due to decreased HOMO-LUMO bandgap [19].

In 2017, CDs were synthesized from citric acid (CA) and urea by the solvothermal method by Tian *et al.* [34]. Water, glycerol, and dimethylformamide (DMF) were used as solvents. CDs synthesized from water, glycerol, and DMF

showed their average diameter as 1.7, 2.8, and 4.5 nm, respectively. Their TEM images and size histogram are shown in **Figure 2.5 (A-C)**. The increase of particle sizes is a result from increasing of the sp^2 -domain. Their absorption bands and fluorescence emission bands were red-shifted with the increase of particle sizes, as shown in **Figure 2.5 (D)**.

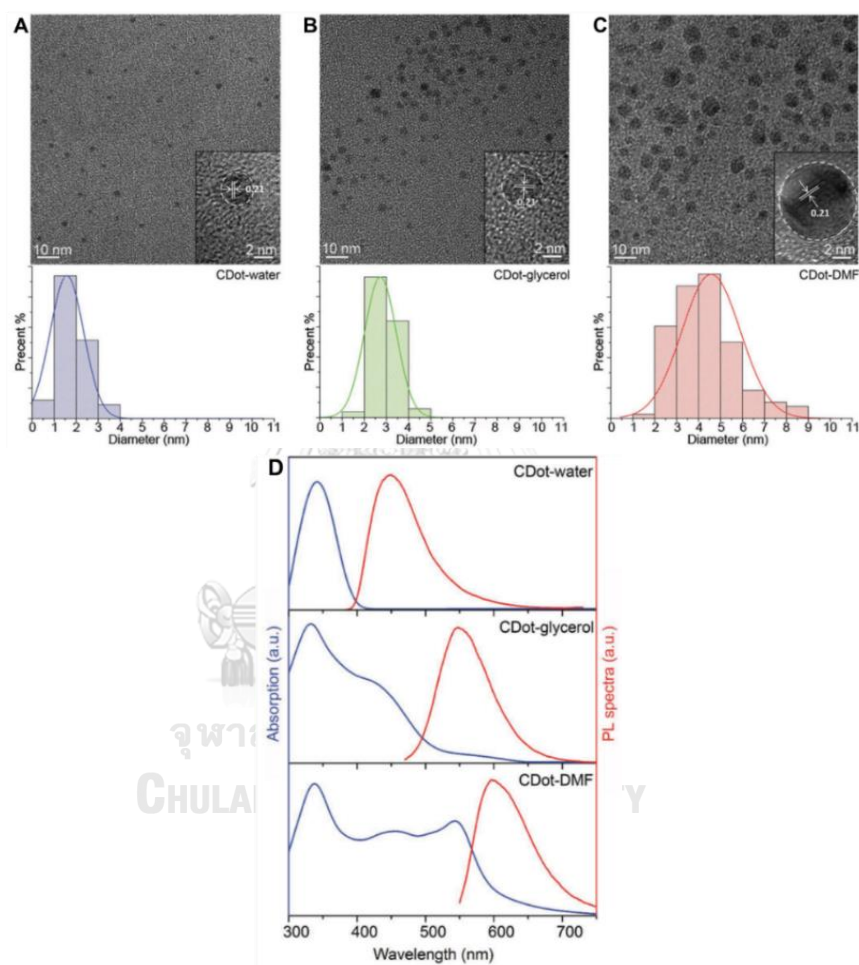


Figure 2.5 (A)-(C) TEM images (top) of CDs synthesized in water, glycerol, and DMF; and their corresponding size histograms (bottom). (D) Absorption and fluorescence emission spectra of CDs were synthesized in water, glycerol, and DMF, respectively, at 360, 420, and 540 nm excitations. Reprinted with permission from ref. [34], Copyright 2017, John Wiley and Sons.

2.5.2 Surface defect state

The surface defect state is frequently used for describing the fluorescence mechanism of CDs. A surface defect influenced by surface oxidation can capture excitons and cause a surface defect state fluorescence [35, 36]. Each surface functional group has a different energy level, leading to a series of emission traps [37-39]. Surface defects are not only oxygen-containing surface functional groups; however, dangling bonds, non-radiative states, and nitrogen-containing functional groups are surface defects also [27].

Ding *et al.* [40] synthesized CDs from urea and *p*-phenylenediamine. Those precursors were treated by hydrothermal method. Crude products were purified by column chromatography which silica was a stationary phase, and the mixture of ethyl acetate and ethanol was a mobile phase. The synthesis and purification process of CDs in Ding's research is shown in **Figure 2.6 (A)**. Images taking under 365 nm UV light and fluorescence emission spectra of each fraction of synthesized CDs are shown in **Figure 2.6 (B)–(C)**. The results show that the polarity of CDs, influenced by their degree of surface oxidation, coincided with fluorescence emission wavelength: higher polarity, higher degree of surface oxidation, higher fluorescence emission wavelength. The red-shift of fluorescence emission wavelength was influenced by decreasing the gap between the highest occupied molecular orbital (HOMO) and the lowest unoccupied molecular orbital (LUMO) caused by their surface oxygen, as shown in **Figure 2.6 (D)**

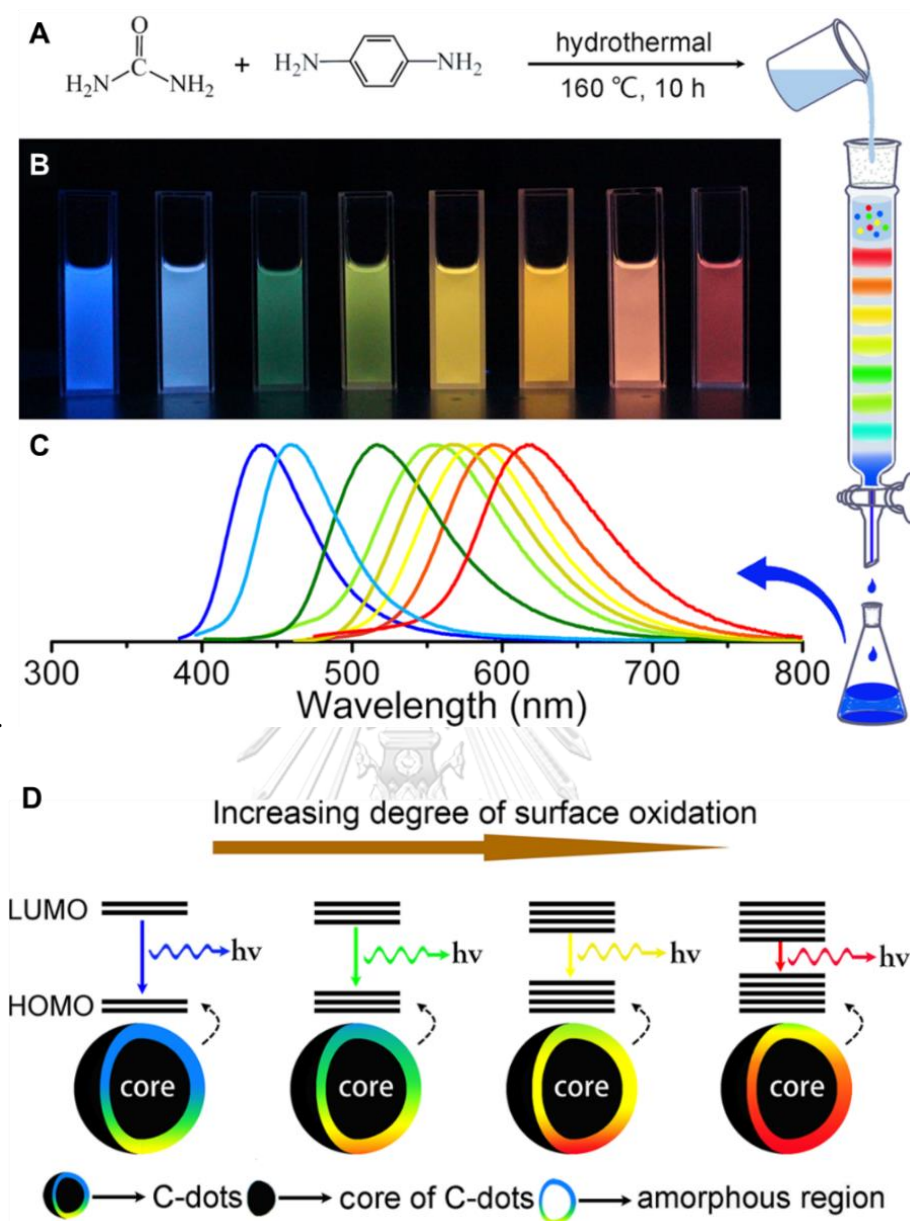


Figure 2.6 (A) Synthesis of CDs in Ding's research. (B) Images that were taken under 365 nm UV light and (C) fluorescence emission spectra of each fraction of CDs. (D) influence of the degree of surface oxidation on their HOMO and LUMO gap. Reprinted with permission from ref. [40], Copyright 2016, American Chemical Society.

2.5.3 Molecular fluorescence

In CDs synthesis, especially bottom-up synthesis, molecular precursors can produce fluorophores [41]. These fluorophores can be attached to the surface of CDs or embedded in the carbon matrix of the core and emit fluorescence along with the core and surface functional groups of CDs [42]. Moreover, the fluorescence emission mechanism can be affected by the interaction between bandgap fluorescence and molecular fluorescence [43].

Song *et al.* [44] synthesized CDs from citric acid and ethylenediamine. Fluorophore (imidazo[1,2-a]pyridine-7-carboxylic acid, 1,2,3,5-tetrahydro-5-oxo-, IPCA) was obtained after CDs purification. CDs which synthesized at low temperature, IPCA is a dominant fluorescence center. When the reaction temperature was increased, IPCA in the system was further carbonized and form as a part of the crystalline carbon core. Thus, CDs prepared with high temperature showed that the dominant fluorescence center was a carbon core.

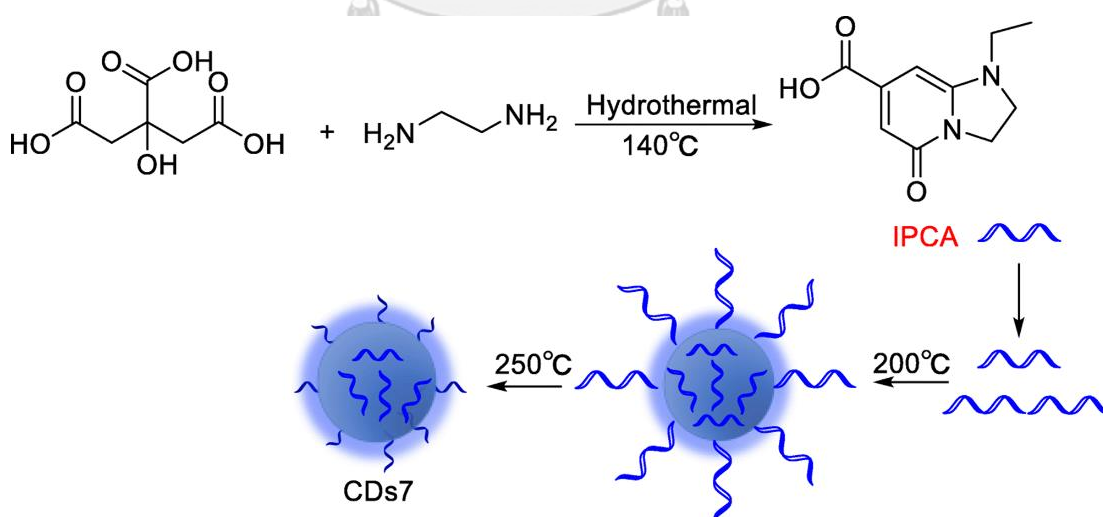


Figure 2.7 Schematic presentation of CDs synthesis in Song's research. Reprinted with permission from ref. [18], Copyright 2019, Springer.

2.5.4 Heteroatom doping

CDs without any modification are usually composed of C and O and emit blue fluorescence with low QYs. Both non-metallic elements, such as nitrogen, phosphorus, and sulfur, and metallic elements, such as copper and manganese, can be dopants of CDs [45]. Doping heteroatoms can improve QYs and tuning their fluorescence emission wavelength. Heteroatoms can be both on the surface and embedded within the carbon core. Surface heteroatoms can improve the yield of radiative recombination by suppressing the original O-states. Heteroatoms in carbon core structure can be tuning fluorescence emission wavelength by changing the initial bandgap. Moreover, the photoluminescence decay lifetime can also be affected by heteroatoms [9].

2.6 Nitrogen-doped carbon dots

Nitrogen is usually used as a dopant for CDs due to its similar atomic radius to carbon [11-13]. Doping nitrogen into CDs skeleton can affect emission wavelength and QY of fluorescence emission [46, 47]. Nitrogen dopant is considered as an n-type dopant that affects Fermi level and optical properties by providing excess electrons [48-51]. The new surface state, so-called N-state, can be produced by doping nitrogen atoms into CDs. N-state can traps electrons, increases the radiative, and suppresses non-radiative recombination, as shown in **Figure 2.8** [52, 53]. The absorption peak of NCDs can be red-shifted due to their decreased bandgap caused by electron cloud activity enhancing [54]. Otyepka and co-workers [55] synthesized NCDs from citric acid and urea by the solvothermal method in formamide media. Synthesized NCDs were separated based on surface charge using ion-exchange column chromatography.

The results showed that the absorption and fluorescence emission were red-shifted when nitrogen contents in NCDs were increased, as shown in **Figure 2.9**. Time-dependent density functional (TD-DFT) calculation suggests that red-shifted in absorption and fluorescence emission caused by the midgap state located between HOMO and LUMO which influenced from nitrogen contents in NCDs.

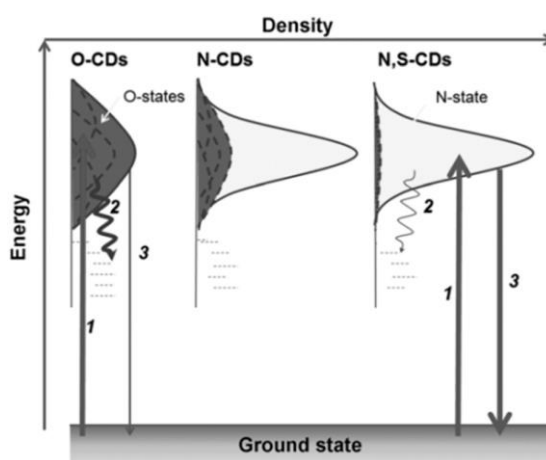


Figure 2.8 Representation for the fluorescent mechanism of O-CDs, N-CDs, and N,S-CDs. 1) Electrons excited from the ground state and trapped by the surface states; 2) excited electrons return to the ground state via a non-radiative route; 3) excited electrons return to the ground state via a radiative route. Reprinted with permission from ref. [52], Copyright 2013, John Wiley and Sons.

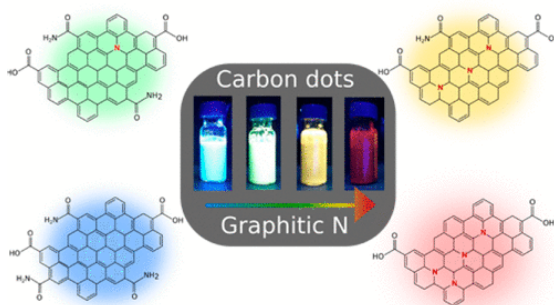


Figure 2.9 Schematic presentation of tunable fluorescence emission with increasing nitrogen content in the graphitic framework. Reprinted with permission from ref. [55], Copyright 2017, American Chemical Society.

CHAPTER III

EXPERIMENTAL SECTION

3.1 Chemicals

Glycine ($C_2H_5NO_2$) and L-tryptophan ($C_{11}H_{12}N_2O_2$) were purchased from Tokyo Chemical Industry Co., Ltd. L-histidine ($C_6H_9N_3O_2$), L-phenylalanine ($C_9H_{11}NO_2$), L-tyrosine ($C_9H_{11}NO_3$), quinine hemisulfate monohydrate ($C_{40}H_{54}N_4O_{10}S$), and hydrochloric acid (HCl) were purchased from Sigma-Aldrich. All chemicals were analytical reagent grade and used as received without any further purification. Milli-Q water obtained Milli-Q system (Millipore, Belford, MA, USA), and deionized water were used as a solvent.

3.2 Synthesis of nitrogen-doped carbon dots

6.25 mmol of amino acids were dissolved in 25 mL 1 M HCl and vigorously stirred until amino acids were dissolved. The amino acid solution was transferred to a Teflon-lined hydrothermal reactor and heated at 200 °C for 12 hours. The hydrothermal reactor was chilled at room temperature. The solution was centrifuged at 15,000 rpm for 30 minutes to eliminate large particles. The supernatant was collected for further characterization.

3.3 Characterizations

3.3.1 Optical properties characterizations

The supernatant collected in 3.2 was dialyzed against deionized water through the dialysis membrane with a cut-off molecular weight of 1,500 Dalton for 12 hours. The solution in the membrane bag was filtrated through a 0.21-micron cellulose filter. The filtrated solution was characterized with 3453 UV-visible spectrophotometer (Agilent) and Cary eclipse fluorescence spectrophotometer (Agilent) to obtain UV-visible and fluorescence spectra, respectively.

The relative fluorescence quantum yield (QY) of His-NCDs, Tyr-NCDs, and Trp-NCDs were determined using quinine hemisulfate monohydrate (QHS) in 0.1 M H₂SO₄, which shows a QY of 0.5777 at the excitation wavelength of 350 nm, as a reference solution. Moreover, L-phenylalanine in deionized water with the QY of 0.024 at the excitation wavelength of 260 nm was used as a reference solution in the QY determination for Phe-NCDs and Gly-NCDs. Reference solutions and dialyzed NCDs samples were diluted to various concentrations. UV-visible absorbance and integrated fluorescence emission intensity were analyzed from both reference and NCDs solutions. UV-visible absorbance of all samples was maintained under 0.1 to avoid the inner filter effect. UV-visible absorbance and integrated fluorescence emission intensity obtained at each concentration were plotted versus each other, and relative QY was calculated using equation 3.1.

$$QY_s = QY_r \left(\frac{m_s}{m_r} \right) \left(\frac{n_s}{n_r} \right)^2 \quad (3.1)$$

Where QY_s is the quantum yield of NCDs, QY_r is the quantum yield of reference, n_s is the refractive indexes of a media of sample, n_r is the refractive indexes of a media of reference, m_s is the gradients obtained from the linear trendline created

from the plotted between UV-visible absorption and integrated fluorescence emission intensity of sample, and m_r is the gradients obtained from the linear trendline created from the plotted between UV-visible absorption and integrated fluorescence emission intensity of reference.

3.3.2 Morphological characterization

Tecnai 20 transmission electron microscope (Philips) was used for determining the particle size. TEM samples can be prepared by neutralizing the solution from **3.2** to prevent the damage of Cu-grid and the instrument caused by acid. Then, filtrate with a 0.21-micron cellulose filter. Filtrated solution will be dropped onto the 200-mesh carbon-coated copper grid and dried under vacuum.

3.3.3 Chemical structure characterization

Fourier-transform infrared spectroscopy was applied to determine the surface functional groups. The solution obtained from **3.2** was dialyzed against deionized water for 48 hours. Then, the dialyzed solution was filtrated through a 0.21-micron cellulose filter. Filtrated solution was freeze-dried until CDs powder was obtained. Powder CDs were characterized using the Nicolet iS5 FTIR spectrometer (Thermo Scientific) with an iD7 ATR accessory.

Raman spectroscopy was used to study the relative amount of crystalline and amorphous carbon in CDs. The solution obtained from **3.2** was dialyzed against deionized water for 12 hours. Then, the dialyzed solution was filtrated through a 0.21-micron cellulose filter. Filtrated solution was dropped on the glass slide, which was enveloped with aluminum foil, and dried in a vacuum. Repeat those steps until there was the layer of NCDs appeared on aluminum foil. Prepared

samples were characterized using the DXR Raman microscope (Thermo Scientific) with a 532-nm excitation laser at a laser power of 2 mW.



CHAPTER IV

RESULTS AND DISCUSSION

4.1 Optical properties of NCDs

We studied optical properties of NCDs to determine their structure and estimate differences of energy gaps between HOMO and LUMO of NCDs which were synthesized from different precursors. Optical properties of 12-hours-dialyzed NCDs were investigated by UV-visible and fluorescence spectroscopy. UV-visible spectra of NCDs are shown in **Figure 4.1**.

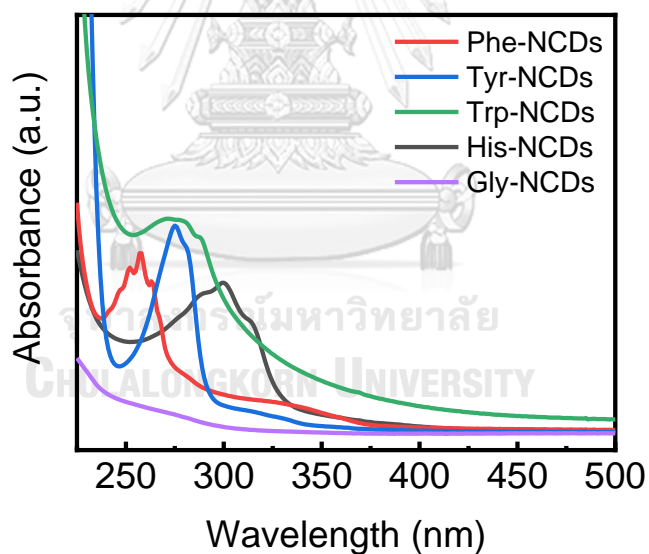


Figure 4.1 UV-visible spectra of synthesized NCDs

All NCDs show two significant absorption regions at 250–300 nm, attributing to $\pi \rightarrow \pi^*$ transition of C=C bond, and at 300–400 nm, attributing to $n \rightarrow \pi^*$ transition of chemical bonds between carbon and heteroatoms such as O and N. Thus,

synthesized NCDs are composed of both graphitic carbon core and surface functional groups.

Fluorescence spectroscopy was applied to investigate the energy gap between HOMO and LUMO, and the width of an additional interband of each NCD. Fluorescence spectra are shown in **Figure 4.2**. The excitation-dependent fluorescence emission was observed when the excitation wavelength was varied from 300–400 nm with an increment of 10 nm. For His-NCDs, Phe-NCDs, and Trp-NCDs, each excitation wavelength results in one emission band.

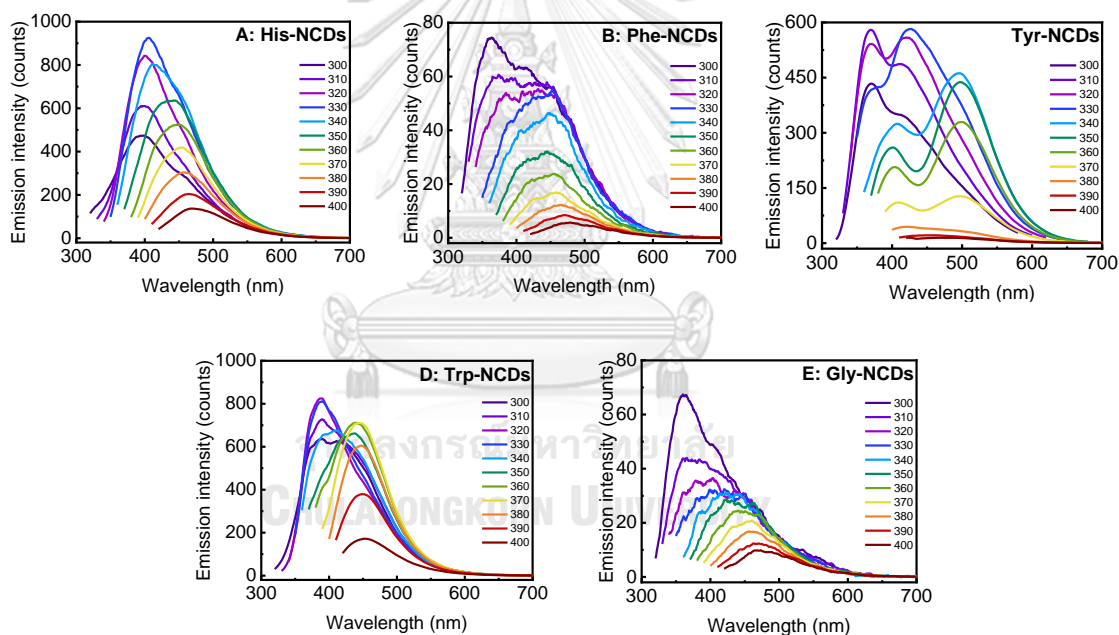


Figure 4.2 Fluorescence emission spectra using various excitation wavelength from 300–400 nm with an increment of 10 nm collected from (A) His-NCDs, (B) Phe-NCDs, (C) Tyr-NCDs, (D) Trp-NCDs, and (E) Gly-NCDs.

However, two fluorescence emission bands can be observed from Tyr-NCDs by one excitation wavelength. Emission peaks are located around 370–380 and 410–430 nm when the excitation wavelength is 300–330 nm. These emissions come from

di-tyrosine and tri/tetra-tyrosine, respectively [56]. Moreover, there are emission peaks at 400–420 and 450–500 nm when the sample is excited with 340–370 nm. These emissions come from tri/tetra-tyrosine and Tyr-NCDs, respectively. Therefore, only emission spectra which are excited with 340–370 nm are considered as fluorescence emission from NCDs.

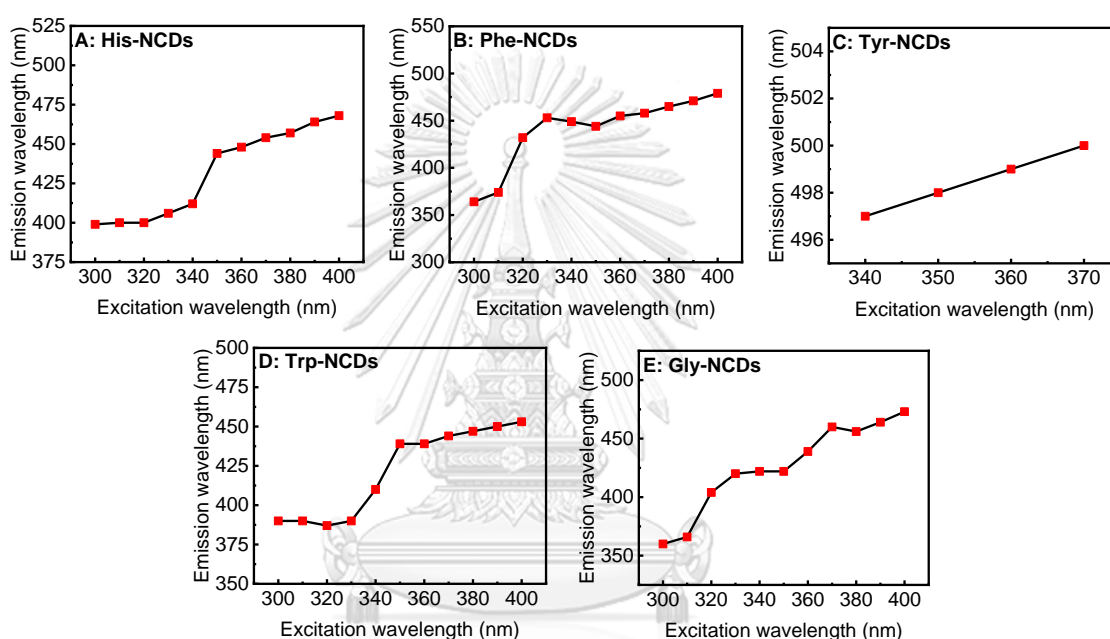


Figure 4.3 Plots between the excitation wavelength and emission wavelength of (A) His-NCDs, (B) Phe-NCDs, (C) Tyr-NCDs, (D) Trp-NCDs, and (E) Gly-NCDs.

Plots between excitation wavelength and emission wavelength of His-NCDs, Phe-NCDs, Trp-NCDs, Tyr-NCDs, and Gly-NCDs are presented in **Figure 4.3**. His-NCDs, Phe-NCDs, Trp-NCDs, and Gly-NCDs show the same trend. There is a red-shift of emission wavelength when the excitation wavelength is increased, which corresponds to previous works about carbon dots [16, 57, 58]. The phenomena observed from His-NCDs, Phe-NCDs, Trp-NCDs, and Gly-NCDs are called

“excitation-dependent fluorescence emission.” A cocktail of different functionalized NCDs contributes to excitation-dependent fluorescence emission.

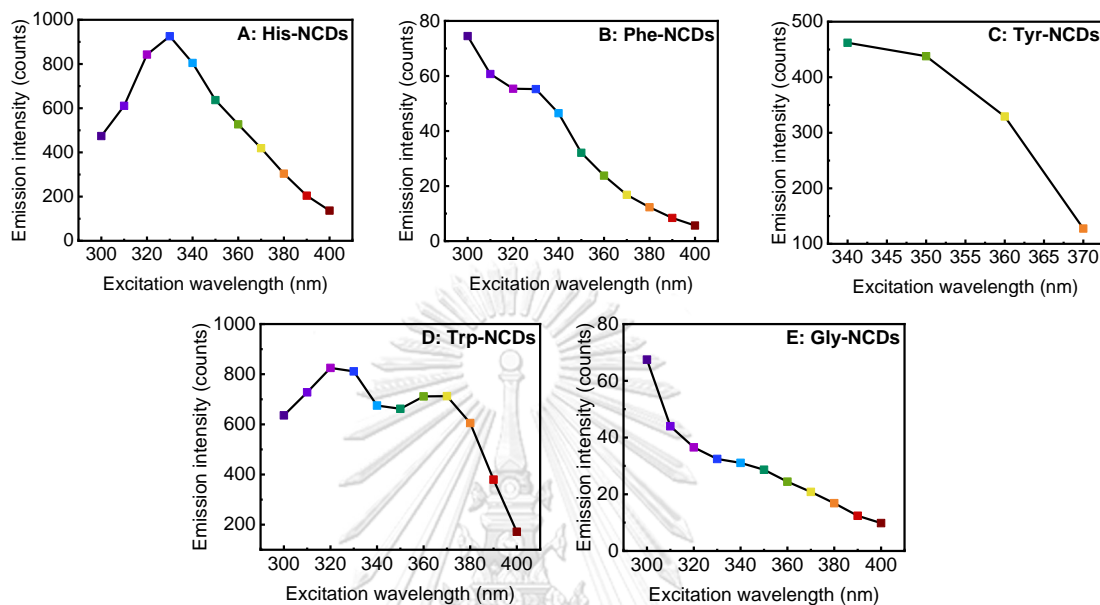


Figure 4.4 Plots between maximum emission intensities and their corresponding excitation wavelength of (A) His-NCDs, (B) Phe-NCDs, (C) Tyr-NCDs, (D) Trp-NCDs, and (E) Gly-NCDs

Plots between maximum emission intensities and their corresponding excitation wavelength in fluorescence emission spectra collected from all types of NCDs are plotted in **Figure 4.4**. Two values were observed from the spectra with the maximum intensity. The first is excitation wavelength inducing NCDs to emit fluorescence at the maximum intensity (λ_{ex}). The second is emission wavelength at the maximum emission intensity (λ_{em}). λ_{ex} of His-NCDs, Tyr-NCDs, and Trp-NCDs are 330, 340, and 320 nm, respectively. λ_{em} of His-NCDs, Tyr-NCDs, and Trp-NCDs are 406, 497, and 387 nm, respectively. For Phe-NCDs and Gly-NCDs, λ_{ex} and λ_{em} , obtained from **Figure 4.4** might not be correct values because those values are not located on the top of a mountain-like plot like other NCDs. Therefore, excitation

wavelength (λ_{ex}) and emission wavelength (λ_{em}) of Phe-NCDs and Gly-NCDs must be determined when the excitation wavelength is below 300 nm are plotted in **Figure 4.5 (A) and (C)**.

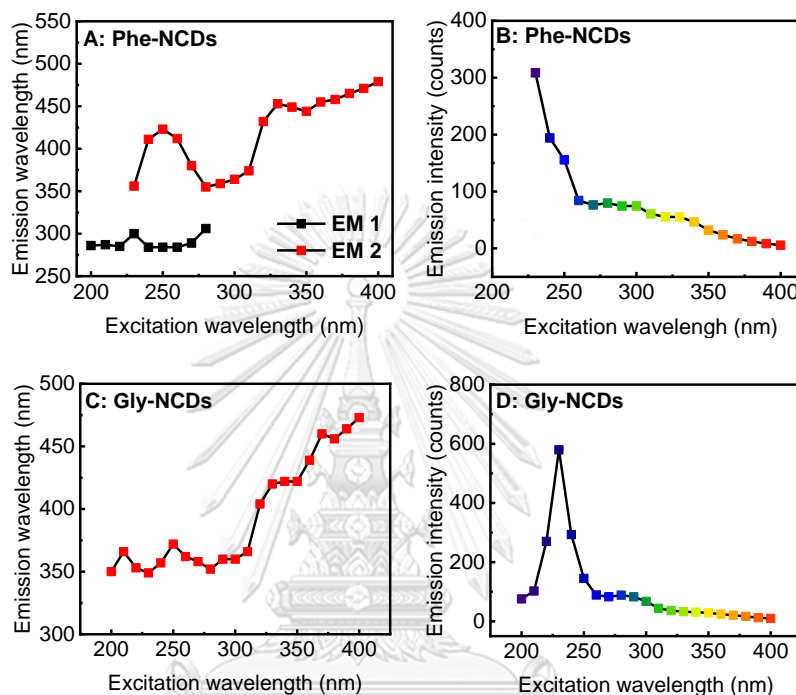


Figure 4.5 Plots between excitation wavelength and emission wavelength of (A) Phe-NCDs and (C) Gly-NCDs. Plots between excitation wavelength and emission intensity of (B) Phe-NCDs and (D) Gly-NCDs

From **Figure 4.5 (A)**, there are two significant emission peaks in the excitation range of 200–280 nm, which are labeled as **EM 1** and **EM 2**, respectively. **EM 1** is an emission from residue L-phenylalanine remaining in the system [59]. Hence, only **EM 2** is considered as an emission from Phe-NCDs. The results show that **EM 2** appeared when the excitation wavelength is 280–400 nm. Therefore, only the relationship between the excitation wavelength and maximum emission intensity in

this excitation range is considered, which is shown in **Figure 4.5 (B)**. From **Figure 4.5 (A)** and **4.5 (B)**, λ_{ex} and λ_{em} of Phe-NCDs are at 230 and 356 nm, respectively.

Gly-NCDs were treated in the same way as Phe-NCDs. The relationship between the excitation and the emission wavelength of Gly-NCDs is shown in **Figure 4.5 (C)**, and the plots between excitation wavelength and the maximum emission intensity are shown in **Figure 4.5 (D)**. **Figures (C)** and **Figures (D)** provide that λ_{ex} and λ_{em} of Gly-NCDs is at 230 and 349 nm, respectively. λ_{ex} and λ_{em} investigated from all NCDs were in **Table 4.1**.

The energy of photons that used to excite electrons and be emitted from electrons could be calculated from λ_{ex} and λ_{em} , which shown in **Table 4.1**, using Planck's equation, as shown in equation 4.1.

$$E = \frac{hc}{\lambda} \quad (4.1)$$

Where E is energy (eV), h is Planck's constant (4.14×10^{-15} eV·s), c is the velocity of light (3.00×10^8 ms⁻¹), and λ is a wavelength (m).

Table 4.1 λ_{ex} , λ_{em} and ΔE obtained from fluorescence spectra of each NCDs

NCDs	λ_{ex} (nm)	λ_{em} (nm)	E_{ex} (eV)	E_{em} (eV)	ΔE (eV)
His-NCDs	330	406	3.76	3.05	0.70
Phe-NCDs	230	356	5.39	3.48	1.91
Tyr-NCDs	340	497	3.65	2.49	1.15
Trp-NCDs	320	387	3.87	3.20	0.67
Gly-NCDs	230	349	5.39	3.55	1.84

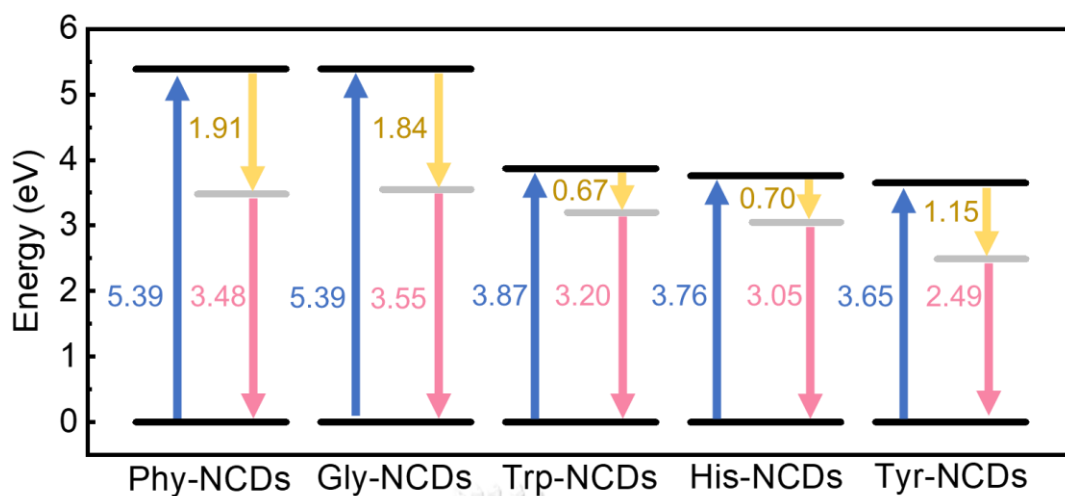


Figure 4.6 The energy gap between HOMO and LUMO, and the width of the additional interband of each NCDs

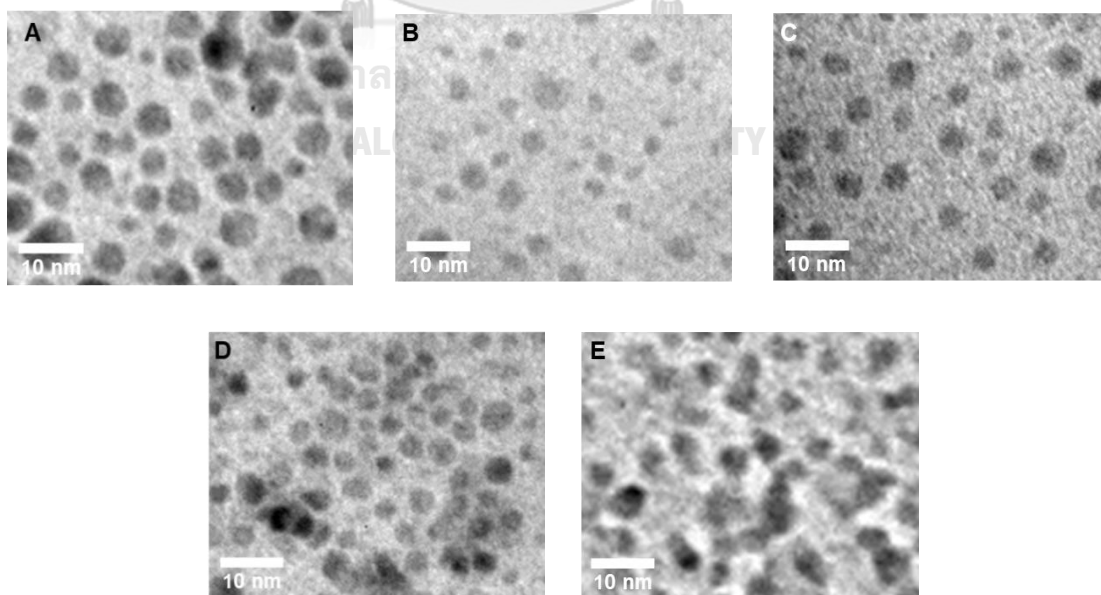
From **Table 4.1**, E_{ex} is represented as excitation energy, which has to be consumed to motivate ground-state-electrons to the excited states, and E_{em} is the energy released in the radiation relaxation step. The difference between E_{ex} and E_{em} , shown as ΔE , is the energy released during non-radiation relaxation induced by the width of the additional interband between HOMO and LUMO. Hence, ΔE values are telling how wide the additional interband is. Phe-NCDs and Gly-NCDs show similar E_{ex} , E_{em} , and ΔE : ~ 5 , ~ 3.5 , and 1.9 eV, respectively. His-NCDs, Tyr-NCDs, and Trp-NCDs show similar E_{ex} : ~ 4 eV. However, E_{em} and ΔE are quite significantly different from His-NCDs and Trp-NCDs. E_{em} and ΔE of His-NCDs and Trp-NCDs is ~ 3 and 0.7 eV, respectively. Meanwhile, E_{em} and ΔE of Tyr-NCDs is ~ 2.5 and ~ 1 eV, respectively. The gap between HOMO and LUMO, and the width of the additional interband of each NCDs can be illustrated in **Figure 4.6** The relative quantum yields of each NCDs are shown in **Table 4.2**.

Table 4.2 Relative quantum yield (QY) of each NCDs

NCDs	QY
His-NCDs	0.033
Phe-NCDs	0.015
Tyr-NCDs	0.047
Trp-NCDs	0.024
Gly-NCDs	0.013

4.2 Morphology and chemical structures of NCDs

Morphology and structure of NCDs were investigated to determine the cause of the differences in optical properties of each NCDs. Morphology of NCDs was monitored by TEM. TEM images of NCDs are shown in **Figure 4.7**, and the histogram of particle size distribution is shown in **Figure 4.8**. **Table 4.5** shows average diameter of each NCDs.

**Figure 4.7** TEM images of (A) His-NCDs, (B) Phe-NCDs, (C) Tyr-NCDs, (D) Trp-NCDs, and (E) Gly-NCDs

All NCDs have a spherical shape with an average diameter of ~ 4 nm. Those results show no significant difference in particle size of NCDs, even synthesized from different precursors. Thus, differences in optical properties are not affected by the quantum confinement effect but possibly by their chemical properties.

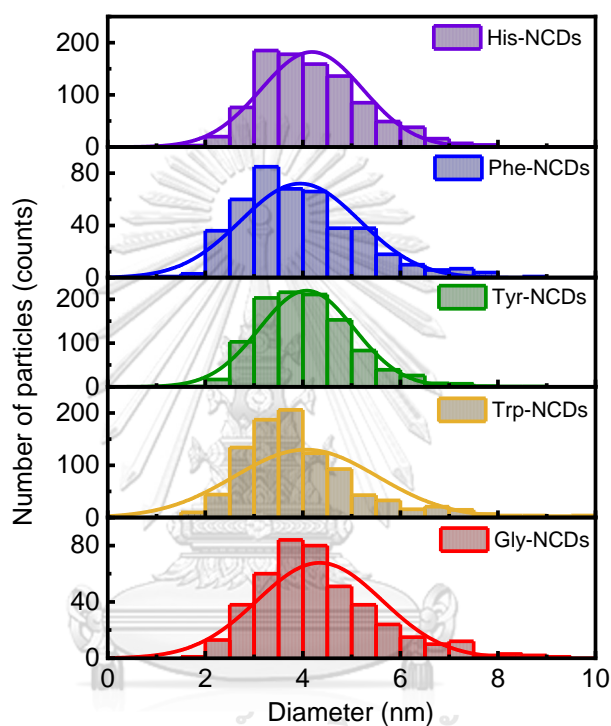


Figure 4.8 Size distribution of NCDs

Table 4.3 Average diameter of each NCDs

NCDs	Average diameter (nm)
His-NCDs	4.19 ± 1.05
Phe-NCDs	3.95 ± 1.22
Tyr-NCDs	4.08 ± 0.97
Trp-NCDs	4.06 ± 1.47
Gly-NCDs	4.34 ± 1.28

FTIR was applied to investigate the data about the surface of NCDs for verification of the doping process and compare the relative amount of each functional group located on the surface of NCDs. **Figure 4.9** shows the FTIR spectra of 48-hours-dialyzed NCDs. Noted that there was no powder of Phe-NCDs left after 48-hours dialysis and freeze-drying, which might cause by their low production yield.

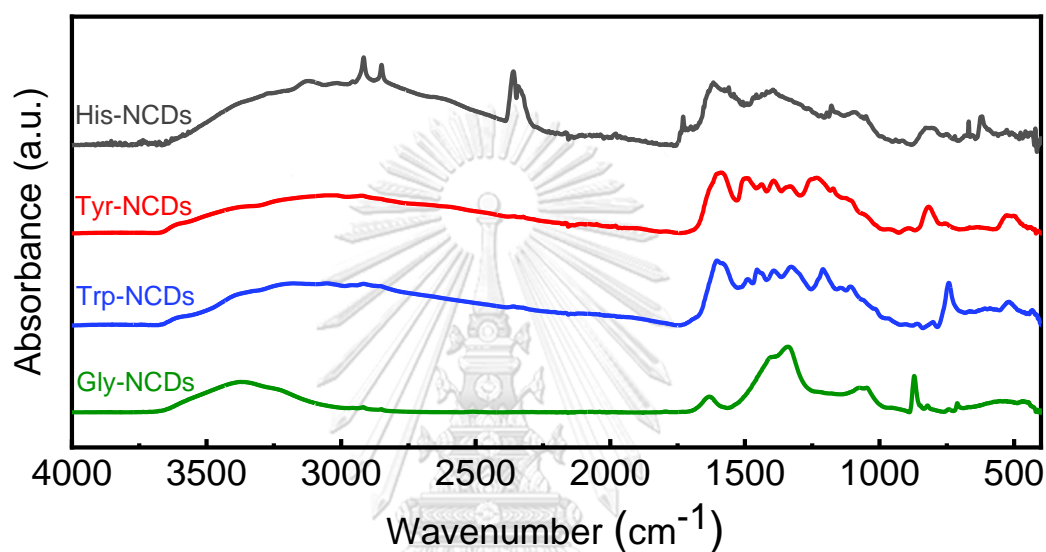


Figure 4.9 FTIR spectra of dialyzed NCDs

FTIR band assignments of the synthesized NCDs are shown in **Table 4.4**. The results show that all NCDs have a broad absorption band around 3100–3500 cm^{-1} , which attributes to O–H and N–H stretching, and also show the absorption peak at $\sim 1600 \text{ cm}^{-1}$ and $\sim 1390 \text{ cm}^{-1}$, assigned to C=O and C–N stretching, respectively. Those indicate the successful doping process. However, absorption peaks at $\sim 2900 \text{ cm}^{-1}$ and $\sim 2850 \text{ cm}^{-1}$ can be observed from all NCDs, attributing to symmetric and asymmetric C–H stretching, respectively. The dominance of those peaks observed from His-NCDs indicates many unfunctionalized areas on their surface.

Table 4.4 FTIR band assignments of different NCDs

Wavenumber (cm ⁻¹)				Assignment	References
His-NCDs	Tyr-NCDs	Trp-NCDs	Gly-NCDs		
Broad absorption at 3100–3500				O–H stretching	[60, 61]
2916	2929	2917	2918	symmetric C–H stretching	[62, 63]
2850	2852	2852	2850	asymmetric C–H stretching	[62, 63]
1617	1587	1603	1631	C=O stretching	[64-66]
1395	1393	1393	1393	C–N stretching	[67-70]
-	1332	1328	1338	C–H bending of –CH ₂	[65, 71-73]
1178	1233	1210	-	C–N stretching and N–H bending (amide III)	[74, 75]
1093	-	-	1074	asymmetric C–O–C stretching	[76]
1050	-	-	1047	symmetric C–O–C stretching	[76]

Although symmetric and asymmetric C–H stretching absorption peaks at ~2900 cm⁻¹ of Tyr-NCDs, Trp-NCDs, and Gly-NCDs are not outstanding, there are C–H on their surface also. Since the absorption peak at ~1330 cm⁻¹ is due to C–H bending of –CH₂ are observed. The amount of N and O on the surface of the NCDs is considered from the relative absorption intensity of C=O and C–N stretching to of C–H bending. Those peaks are located in the wavenumber of 1750–1250 cm⁻¹, as shown in **Figure 4.10**.

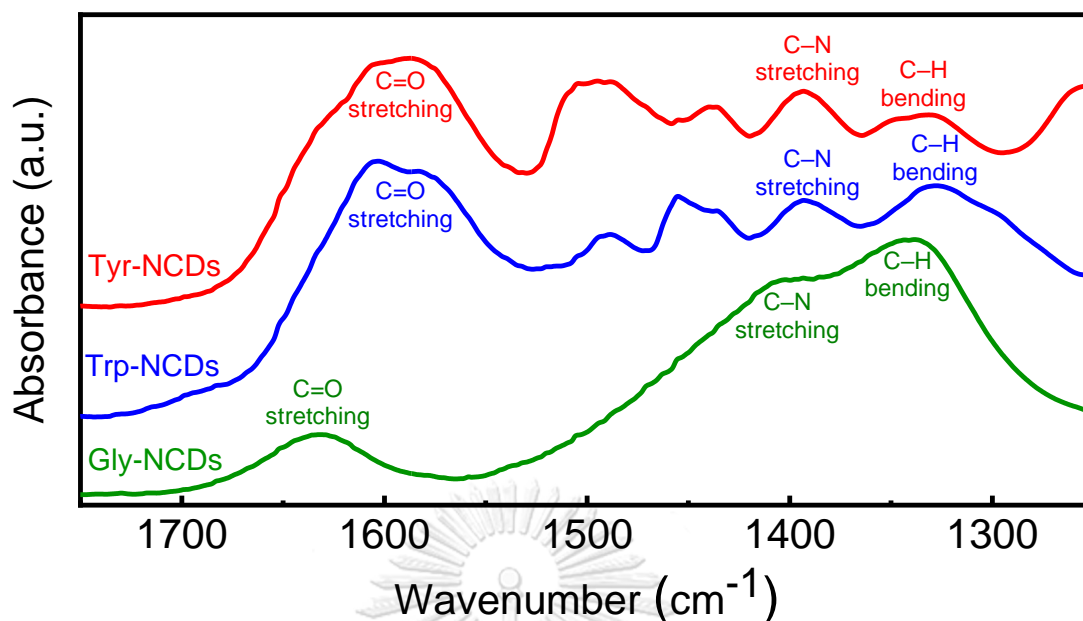


Figure 4.10 FTIR spectra of Tyr-NCDs, Trp-NCDs, and Gly-NCDs in the range of 1750–1250 cm^{-1}

Consider **Figure 4.10**, Gly-NCDs show that the absorbances of C=O and C–N stretching peaks are lower than that of C–H bending peak. For Trp-NCDs, the absorbance of the C–H bending peak is slightly higher than that of the C–N stretching peak while slightly lower than that of the C=O stretching peak. Moreover, C–H bending absorption peak shows the smallest absorbance relative to the C=O stretching and C–N stretching peak. From those results, Tyr-NCDs have higher contents of O and N on the NCDs surface than Trp-NCDs, and Gly-NCDs, respectively, which is consistent with their trend on QY. Tyr-NCDs show the highest QY, while Gly-NCDs show the least QY due to their content of O and N on their surface functional groups.

Although the C–H bending peak cannot be observed from the spectrum of His-NCDs, symmetric and asymmetric C–H stretching peaks, which relate to the unfunctionalized surface, are outstanding. However, those peaks cannot be compared with C=O and C–N stretching peaks in the same spectrum because those C–H

stretching peaks are overlapped with broad O–H stretching peaks. Further analysis of His-NCDs to other NCDs was performed by Raman spectra.

Raman spectra were investigated to observe the relative contents of defects in a graphitic carbon core of NCDs. Raman spectra were investigated from 12-hour-dialyzed NCDs samples. D and G bands centered at 1370 cm^{-1} and 1590 cm^{-1} , respectively, can be observed from all NCDs as shown in **Figure 4.11**. D band arises from symmetry breaking at defects and edges, and G band is caused by in-plane deformation of C–C [77]. The ratio of the integrated intensity of D and G band (I_D/I_G), shown in **Table 4.4**, is ascribed to the ratio of disordered sp^2 and crystalline graphitic carbons, respectively.

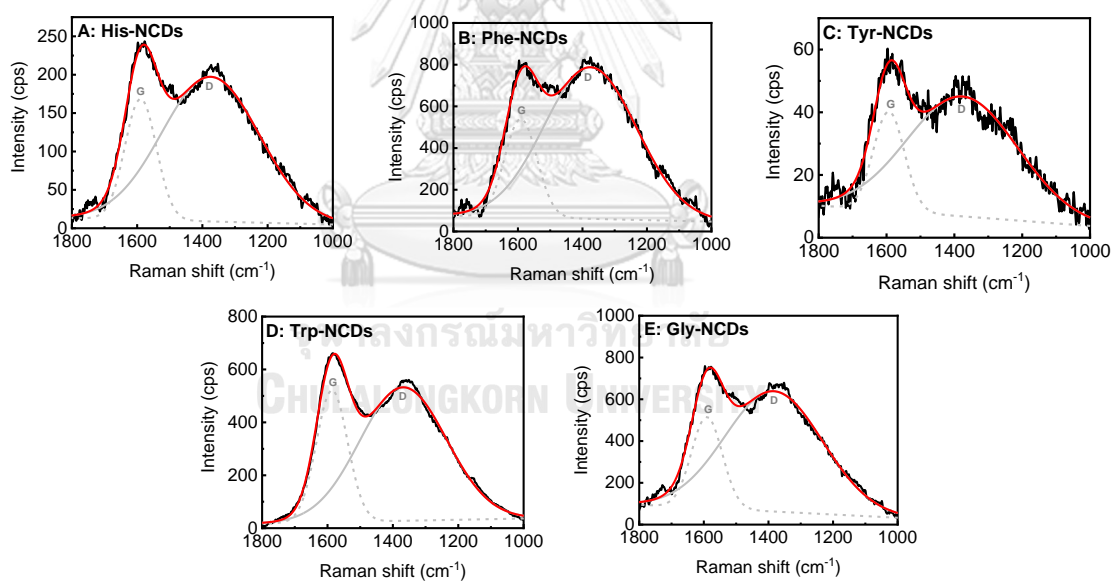


Figure 4.11 Raman spectra of (A) His-NCDs, (B) Phe-NCDs, (C) Tyr-NCDs, (D) Trp-NCDs, and (E) Gly-NCDs.

Table 4.5 Ratio between I_D and I_G of each NCDs

NCDs	I_D/I_G
His-NCDs	2.84 ± 0.56
Phe-NCDs	2.77 ± 0.62
Tyr-NCDs	4.44 ± 0.56
Trp-NCDs	2.69 ± 0.13
Gly-NCDs	3.49 ± 0.82

Gly-NCDs and Phe-NCDs, however, have similar optical properties to each other; however, their I_D/I_G are significantly different. The I_D/I_G of Gly-NCDs and Phe-NCDs are 3.49 and 2.77, respectively. High graphitic carbon network in Phe-NCDs might be induced by the phenyl group of L-phenylalanine. Even Gly-NCDs show a significantly higher value of I_D/I_G than other NCDs, except Tyr-NCDs, their QY is low. FTIR spectrum of Gly-NCDs informs that there are fewer amount of surface functional groups on the Gly-NCDs comparing with other NCDs. Instead of localized on the surface, for Gly-NCDs, heteroatoms might be embedded into a graphitic framework.

I_D/I_G of His-NCDs, Phe-NCDs, and Trp-NCDs are 2.84, 2.77, and 2.69, respectively, which is not significantly different from each other. Meanwhile, I_D/I_G of Tyr-NCDs is 4.44. Molecular structures of those precursors are considered. L-histidine and L-tryptophan are aromatic amino acids, which their sidechain is N-heterocyclic aromatic without any substituent group. Meanwhile, L-tyrosine has a phenyl group connected with a hydroxyl group as a sidechain. N in L-histidine and L-tryptophan are embedded in aromatic groups, making those amino acids have a less

steric effect than L-tyrosine. Moreover, an atomic radius of N is smaller than O. Hence, His-NCDs and Trp-NCDs have smaller defect areas in the carbon core than those in Tyr-NCDs. L-phenylalanine consists of a phenyl ring as a sidechain without any substituent group. Hence their structure is similar to L-histidine and L-tryptophan. Therefore, I_D/I_G of Phe-NCDs is not significantly different from His-NCDs and Trp-NCDs.

Tyr-NCDs has the highest I_D/I_G , which attributes to many defects in the graphitic core of NCDs. Moreover, their FTIR spectrum shows the highest content of surface functional groups. Therefore, Tyr-NCDs has the highest content of heteroatoms which are located on both graphitic carbon core and surface.

4.3 The proposed mechanism of fluorescence emission in NCDs

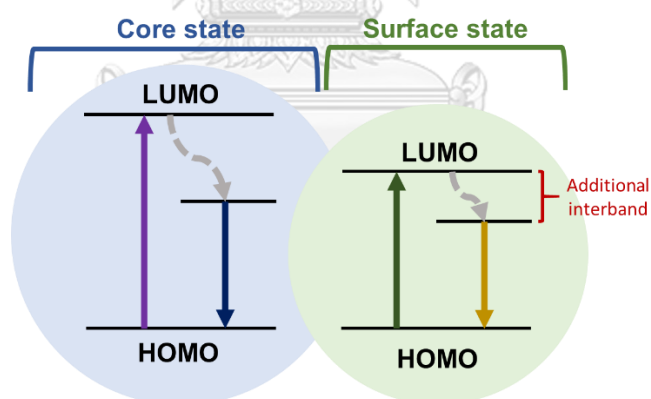


Figure 4.12 Core state and surface state fluorescence emission center

As shown in **Figure 4.7**, NCDs in this research can be classified into two groups using their optical properties. Phe-NCDs and Gly-NCDs have a similar energy gap between HOMO and LUMO, and also the width of an additional interband. Their energy gap between HOMO and LUMO is estimated by the energy of an excitation wavelength, ~ 5 eV, which relates to the excitation energy of electrons in the

conjugated carbon core. Thus, the graphitic carbon core is a fluorescence emission center of Gly-NCDs and Phe-NCDs. The width of an additional interband is influenced by their defect in graphitic structure more than their surface functional groups correspond to their FTIR and Raman spectra.

The other group is Trp-NCDs, His-NCDs, and Tyr-NCDs, which have a similar energy gap between HOMO and LUMO and energy of emission photon. Their HOMO and LUMO energy gap is ~ 4 eV, which relates to the excitation energy of electrons on the surface. Those NCDs show a large amount of surface functional groups, as observed from FTIR spectra. Electron donating groups such as amide and amine can enhance the population of electron which localized on their surface. As a result, their surface functional groups are considered as a fluorescence emission center of those NCDs.

From I_D/I_G observed from Raman spectra, Tyr-NCDs have more defects in graphitic carbon framework than His-NCDs, and Trp-NCDs, respectively. Fluorescence emission wavelength and the width of an additional interband can be influenced by heteroatoms on the surface of the particles or/and heteroatoms which embedded in the graphitic carbon framework. When heteroatoms are increased, fluorescence emission wavelength and the width of an additional interband will be increased too.

For NCDs which fluorescence emission center is a core state like Gly-NCDs and Phe-NCDs, I_D/I_G show that Phe-NCDs is composed of a carbon core with a higher graphitic level than Gly-NCDs. However, an additional interband observed from Phe-NCDs is a bit wider than Gly-NCDs. This might be caused by an increase in

conjugation of a graphitic core which is influenced by phenyl groups of L-phenylalanine.

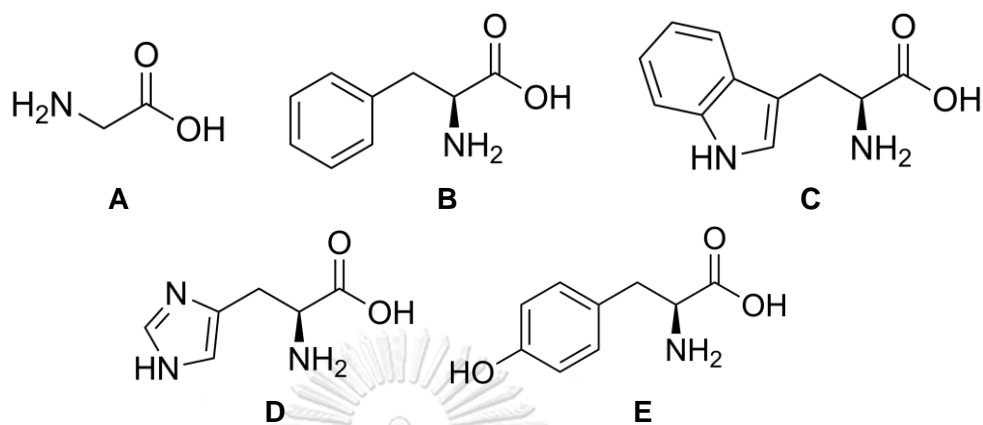
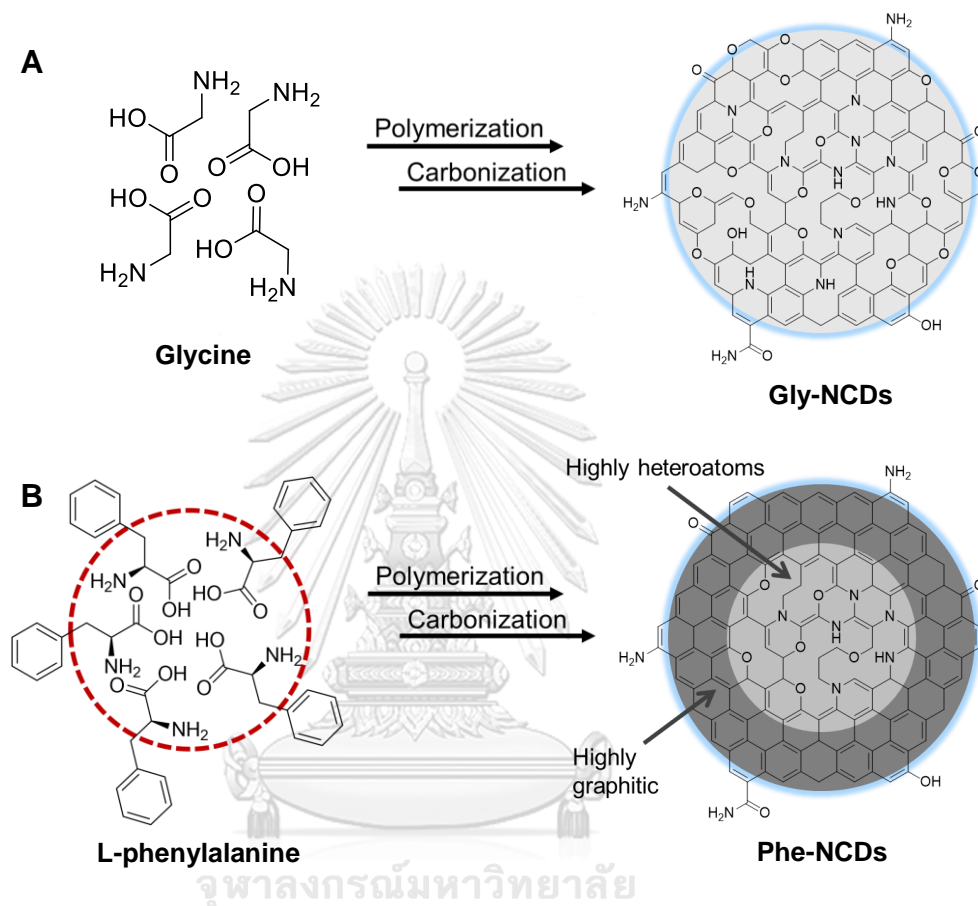


Figure 4.13 Molecular structures of (A) glycine, (B) L-phenylalanine, (C) L-tryptophan, (D) L-histidine, and (E) L-tyrosine

The molecular structures of all precursors, shown in **Figure 4.13**, are considered. The energy gap between HOMO and LUMO of Trp-NCDs and His-NCDs are 3.76 eV and 3.65 eV, respectively. L-histidine and L-tryptophan have nitrogen-containing aromatic structures as a side chain of the molecule. However, two nitrogen atoms embedded in the aromatic ring of L-histidine tend to produce NCDs with more graphitic nitrogen than L-tryptophan, which has only one nitrogen atom in the aromatic ring. The energy gap between HOMO and LUMO of His-NCDs is lower than that of Trp-NCDs because nitrogen atoms implanted in the graphitic core can reduce the energy gap between HOMO and LUMO [78]. Tyr-NCDs show the lowest energy gap between HOMO and LUMO and show the additional interband widest. This might be caused by the hydroxyl group attached to the phenyl ring of L-tyrosine. Those hydroxyl groups can produce NCDs with oxygen atoms in both the graphitic core and on the surface. It is in agreement with the previous study that oxygen atoms

can reduce the energy gap between HOMO and LUMO more than nitrogen [78]. Moreover, the most extensive oxygen contents on the Tyr-NCDs surface can increase the additional interband and the QY.



Scheme 4.1 The proposed formation mechanism of (A) Gly-NCDs and (B) Phe-NCDs

Phe-NCDs and Gly-NCDs show the same trend on the energy gap between HOMO and LUMO, the width of the additional interband, and QY. The molecular structures or precursors are considered—those two amino acids composed of the different side chains. The side chain of glycine and L-phenylalanine is a hydrogen atom and phenyl group, respectively. However, their amino acid backbone is the

same. The similarity in optical properties suggests that their backbone plays an essential role in NCDs production.

The possible formation mechanism is composed of two main steps: polymerization and carbonization, which is in agreement with previous work [58, 69, 79]. First, carbogenic precursors are polymerized. Subsequently, those polymerized precursors are carbonized to be CDs. The possible mechanism of Gly-NCDs is shown in **Scheme 4.1 (A)**. In the polymerization step, glycine molecules are randomly polymerized. Due to their high I_D/I_G and low QY, heteroatoms might be located at the carbon core more than at the surface. In their carbon core, heteroatoms might be uniformly distributed. The proposed formation mechanism of Phe-NCDs is shown in **Scheme 4.1 (B)**. L-phenylalanine is proposed that they undergo the formation step in the same way with glycine. However, a graphitic framework is believed to be influenced by a phenyl group of L-phenylalanine because of their higher I_D/I_G . Since the phenyl group is less reactive, the amino acid backbone might be converged together and then polymerized as NCDs center. Then, those polymerized amino acids were carbonized

His-NCDs, Tyr-NCDs, and Trp-NCDs are assumed that they were polymerized and carbonized in the same way with Gly-NCDs, as shown in **Scheme 4.1 (A)**. From the lower of I_D/I_G than Gly-NCDs, their side chain is supposed to play an essential role in graphitic core formation. Their heteroatoms are located both in the carbon core and on the surface of particles. Their content of surface functional groups might be higher than that of Gly-NCDs, correspond to their FTIR spectra and QY.

CHAPTER V

CONCLUSIONS

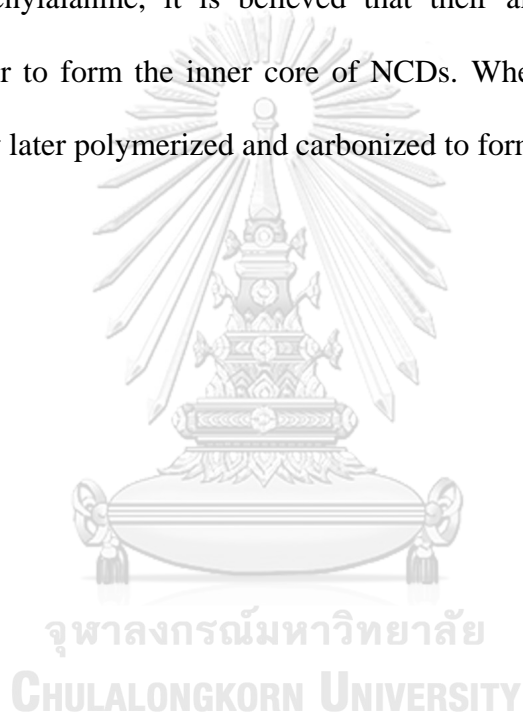
NCDs were successfully synthesized from amino acids under an acidic condition *via the* hydrothermal method at 200°C for 12 hr. Four aromatic amino acids: L-histidine, L-phenylalanine, L-tyrosine, and L-tryptophan, and one aliphatic amino acid: glycine, were used as a precursor. The results show that the chemical structures of precursors can affect optical properties and chemical structures of synthesized NCDs, while their morphologies are similar: spherical shape with a diameter of ~4 nm.

Fluorescence spectroscopy provides that the approximate energy gap between HOMO and LUMO of Phe-NCDs and Gly-NCDs is ~5 eV, and that of His-NCDs, Tyr-NCDs, and Trp-NCDs is ~4 eV. FTIR spectra suggest that Gly-NCDs show fewer surface functional groups than other NCDs. From a high HOMO-LUMO energy gap and low content of surface functional groups, Gly-NCDs and Phe-NCDs are assumed that the core state is their fluorescence emission center. Meanwhile, the fluorescence emission center of His-NCDs, Tyr-NCDs, and Trp-NCDs is assumed to be a surface state due to their lower HOMO-LUMO energy gap high content of surface functional groups.

I_D/I_G obtained from Raman spectra shows that NCDs synthesized from aromatic amino acids, except L-tyrosine, show lower I_D/I_G than NCDs synthesized from glycine. Hence, the aromatic sidechain of precursors can suppress the defect area

in the graphitic carbon core of NCDs. However, Tyr-NCDs show the highest I_D/I_G value due to the highest defect areas in the carbon core influenced by the steric effect of precursors. Although Phe-NCDs and Gly-NCDs show the apparent difference of I_D/I_G , they show similar optical properties.

The formation mechanism of NCDs was proposed. Glycine, L-histidine, L-tyrosine, and L-tryptophan were randomly polymerized and carbonized to produce NCDs. For L-phenylalanine, it is believed that their amino acid backbones are converged together to form the inner core of NCDs. Whereas the less reactivity of phenyl group, they later polymerized and carbonized to form the outer core of NCDs.



REFERENCES

- [1] Y. Liu, H. Huang, W. Cao, B. Mao, Y. Liu, and Z. Kang, "Advances in carbon dots: from the perspective of traditional quantum dots," *Materials Chemistry Frontiers*, 10.1039/D0QM00090F vol. 4, no. 6, pp. 1586-1613, 2020.
- [2] A. N. Emam, S. A. Loutfy, A. A. Mostafa, H. Awad, and M. B. Mohamed, "Cyto-toxicity, biocompatibility and cellular response of carbon dots–plasmonic based nano-hybrids for bioimaging," *RSC Advances*, 10.1039/C7RA01423F vol. 7, no. 38, pp. 23502-23514, 2017.
- [3] S. Liu, N. Zhao, Z. Cheng, and H. Liu, "Amino-functionalized green fluorescent carbon dots as surface energy transfer biosensors for hyaluronidase," *Nanoscale*, 10.1039/C5NR00070J vol. 7, no. 15, pp. 6836-6842, 2015.
- [4] I.-A. Baragau *et al.*, "Continuous hydrothermal flow synthesis of blue-luminescent, excitation-independent nitrogen-doped carbon quantum dots as nanosensors," *Journal of Materials Chemistry A*, 10.1039/C9TA11781D vol. 8, no. 6, pp. 3270-3279, 2020.
- [5] H. Huang *et al.*, "Photocatalytic Polymerization from Amino Acid to Protein by Carbon Dots at Room Temperature," *ACS Applied Bio Materials*, vol. 2, no. 11, pp. 5144-5153, 2019/11/18 2019.
- [6] X. Xu *et al.*, "Electrophoretic Analysis and Purification of Fluorescent Single-Walled Carbon Nanotube Fragments," *Journal of the American Chemical Society*, vol. 126, no. 40, pp. 12736-12737, 2004/10/01 2004.
- [7] Y. Park, Y. Kim, H. Chang, S. Won, H. Kim, and W. Kwon, "Biocompatible nitrogen-doped carbon dots: synthesis, characterization, and application," *Journal of Materials Chemistry B*, 10.1039/D0TB01334J vol. 8, no. 39, pp. 8935-8951, 2020.
- [8] X. Sun and Y. Lei, "Fluorescent carbon dots and their sensing applications,"

TrAC Trends in Analytical Chemistry, vol. 89, pp. 163-180, 2017.

- [9] F. Yan, Z. Sun, H. Zhang, X. Sun, Y. Jiang, and Z. Bai, "The fluorescence mechanism of carbon dots, and methods for tuning their emission color: a review," *Microchimica Acta*, vol. 186, no. 8, p. 583, 2019/07/29 2019.
- [10] Y. Park, J. Yoo, B. Lim, W. Kwon, and S. W. Rhee, "Improving the functionality of carbon nanodots: doping and surface functionalization," *Journal of Materials Chemistry A*, 10.1039/C6TA04813G vol. 4, no. 30, pp. 11582-11603, 2016.
- [11] W.-C. Wu *et al.*, "Nitrogen-doped carbon nanodots prepared from polyethylenimine for fluorometric determination of salivary uric acid," *Microchimica Acta*, vol. 186, no. 3, p. 166, 2019/02/09 2019.
- [12] Y. Liu *et al.*, "Nitrogen doped graphene quantum dots as a fluorescent probe for mercury(II) ions," *Microchimica Acta*, vol. 186, no. 3, p. 140, 2019/02/01 2019.
- [13] L. Wang *et al.*, "A fluorometric aptasensor for bisphenol a based on the inner filter effect of gold nanoparticles on the fluorescence of nitrogen-doped carbon dots," *Microchimica Acta*, vol. 186, no. 1, p. 28, 2018/12/18 2018.
- [14] M. Li *et al.*, "Synthesis and upconversion luminescence of N-doped graphene quantum dots," *Applied Physics Letters*, vol. 101, no. 10, p. 103107, 2012.
- [15] X. Zhai *et al.*, "Highly luminescent carbon nanodots by microwave-assisted pyrolysis," *Chemical Communications*, 10.1039/C2CC33869F vol. 48, no. 64, pp. 7955-7957, 2012.
- [16] H. Huang *et al.*, "Histidine-derived nontoxic nitrogen-doped carbon dots for sensing and bioimaging applications," *Langmuir*, vol. 30, no. 45, pp. 13542-8, Nov 18 2014.
- [17] S. Pei, J. Zhang, M. Gao, D. Wu, Y. Yang, and R. Liu, "A facile hydrothermal approach towards photoluminescent carbon dots from amino acids," *J Colloid*

Interface Sci, vol. 439, pp. 129-33, Feb 1 2015.

- [18] S. Zhu, Y. Song, X. Zhao, J. Shao, J. Zhang, and B. Yang, "The photoluminescence mechanism in carbon dots (graphene quantum dots, carbon nanodots, and polymer dots): current state and future perspective," *Nano Research*, journal article vol. 8, no. 2, pp. 355-381, February 01 2015.
- [19] L. Ai *et al.*, "Insights into photoluminescence mechanisms of carbon dots: Advances and perspectives," *Science Bulletin*, 2020/12/16/ 2020.
- [20] S. Tao, T. Feng, C. Zheng, S. Zhu, and B. Yang, "Carbonized Polymer Dots: A Brand New Perspective to Recognize Luminescent Carbon-Based Nanomaterials," *The Journal of Physical Chemistry Letters*, vol. 10, no. 17, pp. 5182-5188, 2019/09/05 2019.
- [21] F. Yuan, S. Li, Z. Fan, X. Meng, L. Fan, and S. Yang, "Shining carbon dots: Synthesis and biomedical and optoelectronic applications," *Nano Today*, vol. 11, no. 5, pp. 565-586, 2016/10/01/ 2016.
- [22] M. Liu, Y. Xu, F. Niu, J. J. Gooding, and J. Liu, "Carbon quantum dots directly generated from electrochemical oxidation of graphite electrodes in alkaline alcohols and the applications for specific ferric ion detection and cell imaging," *Analyst*, 10.1039/C5AN02231B vol. 141, no. 9, pp. 2657-2664, 2016.
- [23] Q. Zhang, X. Sun, H. Ruan, K. Yin, and H. Li, "Production of yellow-emitting carbon quantum dots from fullerene carbon soot," *Science China Materials*, vol. 60, no. 2, pp. 141-150, 2017/02/01 2017.
- [24] C. Doñate-Buendia, R. Torres-Mendieta, A. Pyatenko, E. Falomir, M. Fernández-Alonso, and G. Mínguez-Vega, "Fabrication by Laser Irradiation in a Continuous Flow Jet of Carbon Quantum Dots for Fluorescence Imaging," *ACS Omega*, vol. 3, no. 3, pp. 2735-2742, 2018/03/31 2018.

- [25] C.-B. Ma *et al.*, "A general solid-state synthesis of chemically-doped fluorescent graphene quantum dots for bioimaging and optoelectronic applications," *Nanoscale*, 10.1039/C5NR01757B vol. 7, no. 22, pp. 10162-10169, 2015.
- [26] J. R. Lakowicz, *Principles of Fluorescence Spectroscopy*. Springer US, 2007.
- [27] J. Gao, M. Zhu, H. Huang, Y. Liu, and Z. Kang, "Advances, challenges and promises of carbon dots," *Inorganic Chemistry Frontiers*, vol. 4, no. 12, pp. 1963-1986, 2017.
- [28] Z. Liu *et al.*, "Improving methane selectivity of photo-induced CO₂ reduction on carbon dots through modification of nitrogen-containing groups and graphitization," *Applied Catalysis B: Environmental*, vol. 232, pp. 86-92, 2018/09/15/ 2018.
- [29] F. Qian, X. Li, L. Tang, S. K. Lai, C. Lu, and S. P. Lau, "Potassium doping: Tuning the optical properties of graphene quantum dots," *AIP Advances*, vol. 6, no. 7, p. 075116, 2016/07/01 2016.
- [30] H. Tao *et al.*, "In Vivo NIR Fluorescence Imaging, Biodistribution, and Toxicology of Photoluminescent Carbon Dots Produced from Carbon Nanotubes and Graphite," *Small*, <https://doi.org/10.1002/sml.201101706> vol. 8, no. 2, pp. 281-290, 2012/01/23 2012.
- [31] M. A. Sk, A. Ananthanarayanan, L. Huang, K. H. Lim, and P. Chen, "Revealing the tunable photoluminescence properties of graphene quantum dots," *Journal of Materials Chemistry C*, 10.1039/C4TC01191K vol. 2, no. 34, pp. 6954-6960, 2014.
- [32] W. Kwon, G. Lee, S. Do, T. Joo, and S.-W. Rhee, "Size-Controlled Soft-Template Synthesis of Carbon Nanodots toward Versatile Photoactive Materials," *Small*, <https://doi.org/10.1002/sml.201301770> vol. 10, no. 3, pp. 506-513, 2014/02/01 2014.
- [33] T. Zhang *et al.*, "The UV absorption of graphene oxide is size-dependent:

- possible calibration pitfalls," *Microchimica Acta*, vol. 186, no. 3, p. 207, 2019/02/28 2019.
- [34] Z. Tian *et al.*, "Full-Color Inorganic Carbon Dot Phosphors for White-Light-Emitting Diodes," *Advanced Optical Materials*, <https://doi.org/10.1002/adom.201700416> vol. 5, no. 19, p. 1700416, 2017/10/01 2017.
- [35] J. Du *et al.*, "Insight into the effect of functional groups on visible-fluorescence emissions of graphene quantum dots," *Journal of Materials Chemistry C*, 10.1039/C6TC00548A vol. 4, no. 11, pp. 2235-2242, 2016.
- [36] X. Zhang *et al.*, "Color-Switchable Electroluminescence of Carbon Dot Light-Emitting Diodes," *ACS Nano*, vol. 7, no. 12, pp. 11234-11241, 2013/12/23 2013.
- [37] H. Yang, F. Li, C. Zou, Q. Huang, and D. Chen, "Sulfur-doped carbon quantum dots and derived 3D carbon nanoflowers are effective visible to near infrared fluorescent probes for hydrogen peroxide," *Microchimica Acta*, vol. 184, no. 7, pp. 2055-2062, 2017/07/01 2017.
- [38] S. Kiran and R. D. K. Misra, "Mechanism of intracellular detection of glucose through nonenzymatic and boronic acid functionalized carbon dots," *Journal of Biomedical Materials Research Part A*, <https://doi.org/10.1002/jbm.a.35421> vol. 103, no. 9, pp. 2888-2897, 2015/09/01 2015.
- [39] Y. Xu, M. Wu, X. Z. Feng, X. B. Yin, X. W. He, and Y. K. Zhang, "Reduced carbon dots versus oxidized carbon dots: photo- and electrochemiluminescence investigations for selected applications," *Chemistry*, vol. 19, no. 20, pp. 6282-8, May 10 2013.
- [40] H. Ding, S.-B. Yu, J.-S. Wei, and H.-M. Xiong, "Full-Color Light-Emitting Carbon Dots with a Surface-State-Controlled Luminescence Mechanism," *ACS Nano*, vol. 10, no. 1, pp. 484-491, 2016/01/26 2016.
- [41] D. Pan, J. Zhang, Z. Li, and M. Wu, "Hydrothermal Route for Cutting Graphene

- Sheets into Blue-Luminescent Graphene Quantum Dots," *Advanced Materials*, <https://doi.org/10.1002/adma.200902825> vol. 22, no. 6, pp. 734-738, 2010/02/09 2010.
- [42] Z. Shen *et al.*, "Microwave-assisted synthesis of cyclen functional carbon dots to construct a ratiometric fluorescent probe for tetracycline detection," *Journal of Materials Chemistry C*, 10.1039/C8TC02982B vol. 6, no. 36, pp. 9636-9641, 2018.
- [43] C. Hu, T.-R. Su, T.-J. Lin, C.-W. Chang, and K.-L. Tung, "Yellowish and blue luminescent graphene oxide quantum dots prepared via a microwave-assisted hydrothermal route using H₂O₂ and KMnO₄ as oxidizing agents," *New Journal of Chemistry*, 10.1039/C7NJ03337K vol. 42, no. 6, pp. 3999-4007, 2018.
- [44] Y. Song *et al.*, "Investigation from chemical structure to photoluminescent mechanism: a type of carbon dots from the pyrolysis of citric acid and an amine," *Journal of Materials Chemistry C*, 10.1039/C5TC00813A vol. 3, no. 23, pp. 5976-5984, 2015.
- [45] B. B. Chen, M. L. Liu, C. M. Li, and C. Z. Huang, "Fluorescent carbon dots functionalization," *Advances in Colloid and Interface Science*, vol. 270, pp. 165-190, 2019/08/01/ 2019.
- [46] Y. Wang, Q. Zhuang, and Y. Ni, "Facile Microwave-Assisted Solid-Phase Synthesis of Highly Fluorescent Nitrogen-Sulfur-Codoped Carbon Quantum Dots for Cellular Imaging Applications," *Chemistry – A European Journal*, <https://doi.org/10.1002/chem.201501723> vol. 21, no. 37, pp. 13004-13011, 2015/09/07 2015.
- [47] H. Zhang *et al.*, "Solid-Phase Synthesis of Highly Fluorescent Nitrogen-Doped Carbon Dots for Sensitive and Selective Probing Ferric Ions in Living Cells," *Analytical Chemistry*, vol. 86, no. 19, pp. 9846-9852, 2014/10/07 2014.
- [48] S. Chandra, D. Laha, A. Pramanik, A. Ray Chowdhuri, P. Karmakar, and S. K.

- Sahu, "Synthesis of highly fluorescent nitrogen and phosphorus doped carbon dots for the detection of Fe³⁺ ions in cancer cells," *Luminescence*, <https://doi.org/10.1002/bio.2927> vol. 31, no. 1, pp. 81-87, 2016/02/01 2016.
- [49] Y. Wang and A. Hu, "Carbon quantum dots: synthesis, properties and applications," *Journal of Materials Chemistry C*, vol. 2, no. 34, p. 6921, 2014.
- [50] Y.-Q. Zhang *et al.*, "One-pot synthesis of N-doped carbon dots with tunable luminescence properties," *Journal of Materials Chemistry*, 10.1039/C2JM32973E vol. 22, no. 33, pp. 16714-16718, 2012.
- [51] P. Ayala, R. Arenal, A. Loiseau, A. Rubio, and T. Pichler, "The physical and chemical properties of heteronanotubes," *Reviews of Modern Physics*, vol. 82, no. 2, pp. 1843-1885, 06/09/ 2010.
- [52] Y. Dong *et al.*, "Carbon-Based Dots Co-doped with Nitrogen and Sulfur for High Quantum Yield and Excitation-Independent Emission," *Angewandte Chemie International Edition*, vol. 52, no. 30, pp. 7800-7804, 2013/07/22 2013.
- [53] D. Qu *et al.*, "Formation mechanism and optimization of highly luminescent N-doped graphene quantum dots," *Scientific Reports*, vol. 4, no. 1, p. 5294, 2014/06/18 2014.
- [54] X. Li, S. Zhang, S. A. Kulinich, Y. Liu, and H. Zeng, "Engineering surface states of carbon dots to achieve controllable luminescence for solid-luminescent composites and sensitive Be²⁺ detection," *Scientific Reports*, Article vol. 4, 2014, Art. no. 4976.
- [55] K. Holá *et al.*, "Graphitic Nitrogen Triggers Red Fluorescence in Carbon Dots," *ACS Nano*, vol. 11, no. 12, pp. 12402-12410, 2017/12/26 2017.
- [56] E. Sitkiewicz, J. Olędzki, J. Poznanski, and M. Dadlez, "Di-Tyrosine Cross-Link Decreases the Collisional Cross-Section of A β Peptide Dimers and Trimers in

- the Gas Phase: An Ion Mobility Study," *PloS one*, vol. 9, p. e100200, 06/19 2014.
- [57] S. Pandit, P. Behera, J. Sahoo, and M. De, "In Situ Synthesis of Amino Acid Functionalized Carbon Dots with Tunable Properties and Their Biological Applications," *ACS Applied Bio Materials*, vol. 2, no. 8, pp. 3393-3403, 2019/08/19 2019.
- [58] J. Yang, W. Chen, X. Liu, Y. Zhang, and Y. Bai, "Hydrothermal synthesis and photoluminescent mechanistic investigation of highly fluorescent nitrogen doped carbon dots from amino acids," *Materials Research Bulletin*, vol. 89, pp. 26-32, 2017.
- [59] A. P. Demchenko, *Ultraviolet Spectroscopy of Proteins*, 1 ed. Berlin, Heidelberg: Springer, 1986, pp. XI, 312.
- [60] Z. Wang *et al.*, "Facile construction of carbon dots via acid catalytic hydrothermal method and their application for target imaging of cancer cells," *Nano Research*, vol. 9, no. 1, pp. 214-223, 2016/01/01 2016.
- [61] Y. Zheng *et al.*, "A facile approach for the synthesis of highly luminescent carbon dots using vitamin-based small organic molecules with benzene ring structure as precursors," *RSC Advances*, 10.1039/C5RA14720D vol. 5, no. 110, pp. 90245-90254, 2015.
- [62] A. Dager, T. Uchida, T. Maekawa, and M. Tachibana, "Synthesis and characterization of Mono-disperse Carbon Quantum Dots from Fennel Seeds: Photoluminescence analysis using Machine Learning," *Scientific Reports*, vol. 9, no. 1, p. 14004, 2019/09/30 2019.
- [63] N. Arsalani, P. Nezhad-Mokhtari, and E. Jabbari, "Microwave-assisted and one-step synthesis of PEG passivated fluorescent carbon dots from gelatin as an efficient nanocarrier for methotrexate delivery," *Artificial Cells, Nanomedicine*,

and Biotechnology, vol. 47, no. 1, pp. 540-547, 2019/12/04 2019.

- [64] H. Liu, Z. He, L. P. Jiang, and J. J. Zhu, "Microwave-assisted synthesis of wavelength-tunable photoluminescent carbon nanodots and their potential applications," *ACS Appl Mater Interfaces*, vol. 7, no. 8, pp. 4913-20, Mar 4 2015.
- [65] G. Socrates, "Infrared and Raman characteristic group frequencies : tables and charts," 2001.
- [66] D. Wu *et al.*, "Fluorometric determination and imaging of glutathione based on a thiol-triggered inner filter effect on the fluorescence of carbon dots," *Microchimica Acta*, vol. 184, no. 7, pp. 1923-1931, 2017/07/01 2017.
- [67] H. Yang *et al.*, "Hydrophobic carbon dots with blue dispersed emission and red aggregation-induced emission," *Nature Communications*, vol. 10, no. 1, p. 1789, 2019/04/17 2019.
- [68] B. Zhi *et al.*, "Investigation of phosphorous doping effects on polymeric carbon dots: Fluorescence, photostability, and environmental impact," *Carbon*, vol. 129, pp. 438-449, 2018/04/01/ 2018.
- [69] Y.-W. Zeng *et al.*, "N, S co-doped carbon dots with orange luminescence synthesized through polymerization and carbonization reaction of amino acids," *Applied Surface Science*, vol. 342, pp. 136-143, 2015/07/01/ 2015.
- [70] K. Jiang, S. Sun, L. Zhang, Y. Wang, C. Cai, and H. Lin, "Bright-Yellow-Emissive N-Doped Carbon Dots: Preparation, Cellular Imaging, and Bifunctional Sensing," *ACS Applied Materials & Interfaces*, vol. 7, no. 41, pp. 23231-23238, 2015/10/21 2015.
- [71] K. Belbachir, R. Noreen, G. Gouspillou, and C. Petibois, "Collagen types analysis and differentiation by FTIR spectroscopy," *Analytical and Bioanalytical Chemistry*, vol. 395, no. 3, pp. 829-837, 2009/10/01 2009.

- [72] V. Samouillan *et al.*, "Conformational and thermal characterization of left ventricle remodeling post-myocardial infarction," *Biochimica et Biophysica Acta (BBA) - Molecular Basis of Disease*, vol. 1863, no. 6, pp. 1500-1509, 2017/06/01/ 2017.
- [73] Y. J. Phua, W. S. Chow, and Z. A. Mohd Ishak, "Reactive processing of maleic anhydride-grafted poly(butylene succinate) and the compatibilizing effect on poly(butylene succinate) nanocomposites," *Express Polymer Letters*, vol. 7, no. 4, pp. 340-354, 2013.
- [74] Z. S. S. Júnior *et al.*, "Effect of papain-based gel on type I collagen - spectroscopy applied for microstructural analysis," *Scientific Reports*, vol. 5, no. 1, p. 11448, 2015/06/23 2015.
- [75] P. L. Heseltine, J. Hosken, C. Agboh, D. Farrar, S. Homer-Vanniasinkam, and M. Edirisinghe, "Fiber Formation from Silk Fibroin Using Pressurized Gyration," *Macromolecular Materials and Engineering*, <https://doi.org/10.1002/mame.201800577> vol. 304, no. 1, p. 1800577, 2019/01/01 2019.
- [76] A. F. Shaikh, M. S. Tamboli, R. H. Patil, A. Bhan, J. D. Ambekar, and B. B. Kale, "Bioinspired Carbon Quantum Dots: An Antibiofilm Agents," *J Nanosci Nanotechnol*, vol. 19, no. 4, pp. 2339-2345, Apr 1 2019.
- [77] E. Dervishi, Z. Ji, H. Htoon, M. Sykora, and S. K. Doorn, "Raman spectroscopy of bottom-up synthesized graphene quantum dots: size and structure dependence," *Nanoscale*, 10.1039/C9NR05345J vol. 11, no. 35, pp. 16571-16581, 2019.
- [78] J. Yu *et al.*, "Luminescence Mechanism of Carbon Dots by Tailoring Functional Groups for Sensing Fe³⁺ Ions," *Nanomaterials*, vol. 8, no. 4, 2018.
- [79] C. Xia *et al.*, "Hydrothermal Addition Polymerization for Ultrahigh-Yield Carbonized Polymer Dots with Room Temperature Phosphorescence via

Nanocomposite," *Chemistry – A European Journal*,
<https://doi.org/10.1002/chem.201802712> vol. 24, no. 44, pp. 11303-11308,
2018/08/06 2018.



VITA

NAME NATTAPON SIENGDUNG

DATE OF BIRTH 8 August 1994

PLACE OF BIRTH Uttaradit

**INSTITUTIONS
ATTENDED** Chulalongkorn University

HOME ADDRESS 21/1 Village No. 6, Pasao Subdistrict
Muang District, Uttaradit, Thailand



จุฬาลงกรณ์มหาวิทยาลัย
CHULALONGKORN UNIVERSITY